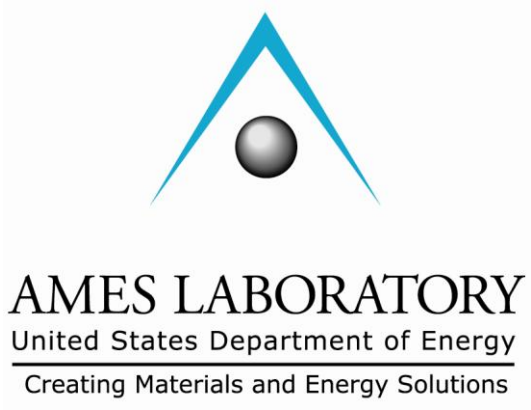

IS-5191

System Cost Analysis for an Interior Permanent Magnet Motor

August 2008

Peter Campbell
Consultant

Ames Laboratory
Iowa State University
Ames, Iowa 50011

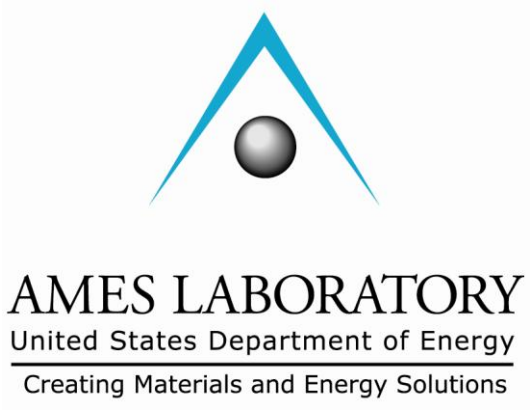

IS-5191

System Cost Analysis for an Interior Permanent Magnet Motor

August 2008

Peter Campbell
Consultant

Prepared for
The U.S. Department of Energy
Office of Energy Science
Ames Laboratory

Work Performed Under Contract No. **DE-AC02-07CH11358**

DISCLAIMER

Final Report
submitted to

Ames Laboratory,

Iowa State University

System Cost Analysis for an Interior Permanent Magnet Motor

by

Peter Campbell, B.Sc., M.A., Ph.D.

August, 2008

TABLE OF CONTENTS

List of Tables

List of Figures

1: INTRODUCTION

1.1: BACKGROUND

The objective of this program is to provide an assessment of the cost structure for an *interior permanent magnet* ("IPM") motor which is designed to meet the 2010 FreedomCAR specification[1]. The program is to evaluate the range of viable permanent magnet materials for an IPM motor, including sintered and bonded grades of rare earth magnets. The study considers the benefits of key processing steps, alternative magnet shapes and their assembly methods into the rotor (including magnetization), and any mechanical stress or temperature limits. The motor's costs are estimated for an annual production quantity of 200,000 units, and are broken out into such major components as magnetic raw materials, processing and manufacturing. But this is essentially a feasibility study of the motor's electromagnetic design, and is not intended to include mechanical or thermal studies as would be done to work up a selected design for production.

1.2: MOTOR SPECIFICATION

It was agreed that the model would be based upon the final IPM motor design which was developed by UQM Technologies Inc. as detailed in their Final Report[2]. Its report adopts and reiterates the FreedomCAR specification as a design specification for the UQM motor, some important requirements of which are summarized in Table 1.

Table 1: Advanced traction motor specifications

Requirement	Specification
Nominal speed (rev/min)	10,000
Peak power at 20% of max. speed for 18 sec. (kW)	55
Battery operating voltage (Vdc)	200-450; nominal: 325
Maximum motor current (A)	400
Characteristic current (Ψ_{mag}/L_d) (A)	<400
Back-e.m.f. at 100% max. speed, peak line-to-line (V)	<600
Efficiency at 10-100% max. speed for 20% rated torque	>93%
Peak power-to-weight ratio for active materials (kW/kg)	>2.75
Peak power-to-vol. ratio for active materials (kW/liter)	>12.5
Motor cost of active materials at peak power ($/kW)	<3.2
Life (years)	>15
Ambient (outside container) operating temperature (^oC)	-40 to +105

[1] *Electrical and Electronics Technical Team Roadmap*, FreedomCAR Fuel Partnership, November 2006.
[2] *Advanced Traction Drive Motor Development Phase 1*, UQM Technologies, September 2006.

UQM interprets the peak power requirement to mean that the motor should develop 55 kW output power from 2,000 to 10,000 rev/min and 262.65 Nm torque at and below 2,000 rev/min, which Figure 1 shows graphically. Furthermore, UQM explains that this peak operating profile is required over the entire voltage range, so most critically the motor must be designed to develop this at the minimum 200V supply and 400A phase current. The requirement for efficiency to exceed 93% is to occur at 20% of rated torque (i.e. 262 x 0.2 = 52 Nm) from 1,000 to 10,000 rev/min, the operating profile for this calculation being shown in Figure 2.

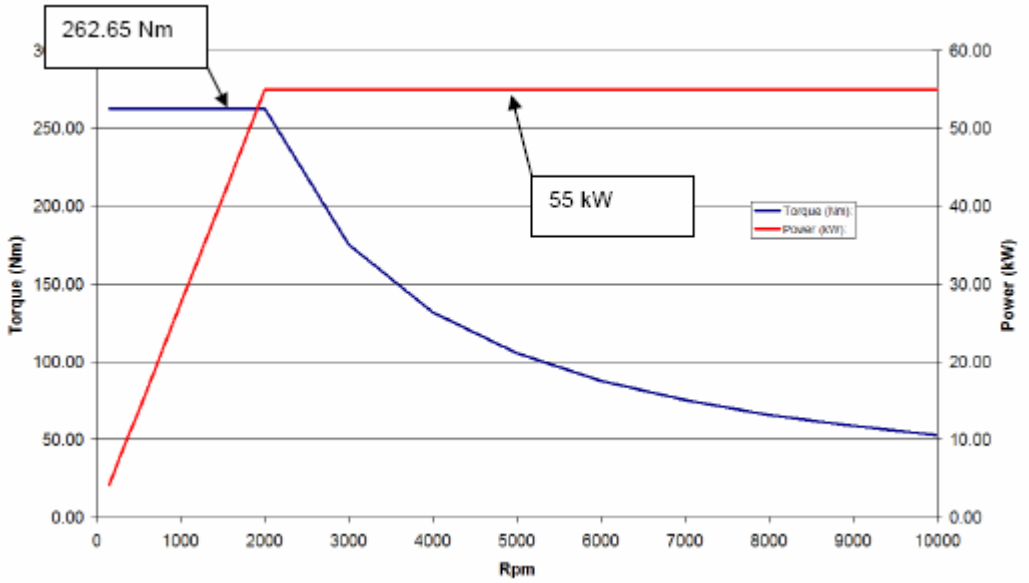

Fig. 1: Peak operating profile (from UQM report)

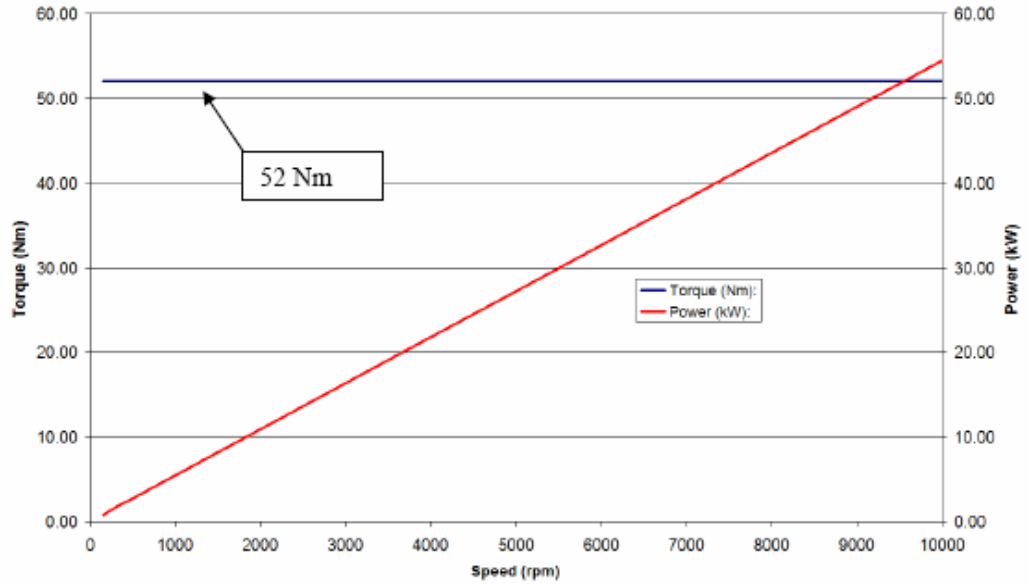

Fig. 2: Operating profile for efficiency (from UQM report)

The “active materials” referenced in Table 1 consist of the stator core, rotor core, stator winding and magnets, and thus correspond with the components which constitute the motor’s “electromagnetic” design of the present study. Peak power of 55 kW means that the maximum weight of these active materials must be 20 kg, their maximum volume must be 4.4 liters, and their total cost should not exceed $176.

1.3: SUMMARY

The first step in the present program involved modeling the benchmark UQM motor design using finite element analysis, which showed that it would not function quite correctly as planned as a hybrid between a permanent magnet motor and a reluctance motor. The constant power feature of the peak operating profile (Figure 1) should be achieved by field weakening, for which it was found that the original sintered NdFeB magnets were slightly too thick. A suitable grade was chosen to operate at the required 160^{o}C with much reduced magnet volume compared to the original, and a new optimized IPM motor design was produced which met the required performance goals with a good margin of safety for the rotor’s integrity at maximum speed. An alternative design was also found to be feasible with anisotropic compression-molded NdFeB magnets using powder made by the “HDDR” process method. Both of the foregoing employed a rotor layout with each pole comprising magnets located in a single U-shaped slot, but a further alternative using isotropic injection-molded NdFeB would require significantly more magnet material distributed into two U-shaped slots per pole and a much longer rotor which far exceeds the power-to-weight and power-to-volume ratios required for this motor. The motor specifications given in Table 1 required the peak power-to-weight ratio for active materials to be >2.75 kW/kg, which is met by both of the viable alternatives for the new IPM motor design as summarized in Table 2.

Table 2: Comparison of active materials per motor in viable new designs

	New design, sintered NdFeB	New design, compression-molded NdFeB
Weight of magnets:	0.65 kg	1.39 kg
Total weight of active materials:	19.12 kg	19.09 kg
Peak power-to-weight ratio for active materials:	2.88 kW/kg	2.88 kW/kg
Cost of magnets:	$59.26	$54.45
Total cost of active materials:	$172.92	$163.68

Around the 160^{o}C temperature of interest, the grade of sintered NdFeB we selected has a greater safety margin with respect to its thermal stability than does the bonded NdFeB using anisotropic HDDR powder. However to do this, sintered NdFeB contains slightly more neodymium, much more dysprosium and

some cobalt. Our studies found that prices of the rare earth elements appear to have stabilized now at relatively high historical levels, and are expected to stay there for the foreseeable future. Factoring in a greater weight but lower manufacturing cost for the compression-molded magnets, this design offers a slightly lower overall magnet cost than with sintered NdFeB as shown in Table 2 using quotations from approved suppliers at quantities of 200,000 motors per year. The corresponding total cost of active materials shows that both new IPM motor designs meet the target of <$176.

We have also studied new materials developments to see if any other grades of sintered or bonded magnet can meet the IPM motor requirements. Interestingly, in our review of raw materials price trends it was found that cobalt is projected fall to around $25/kg by 2015, in which case sintered samarium-cobalt may become a viable alternative to sintered NdFeB. We have noted that Ames Laboratory has developed an alloy with improved temperature stability for use in bonded NdFeB magnets, and if it were possible to moderate its dysprosium content while developing grain alignment to turn this into an *anisotropic* powder, it would be certainly be preferable to HDDR powder as a compression-molded magnet for the IPM motor.

2: BENCHMARK MOTOR

2.1: UQM FINAL DESIGN PARAMETERS

Particulars of the final IPM motor designed by UQM Technologies were obtained or inferred from their Final Report[2]. The major dimensions from Table 12 of its report are given in Table 3 here, while details had to be scaled from their drawing (Figure 3).

Table 3: UQM final motor design parameters

Outer stator diameter (in.)	8.70
Inner stator diameter (in.)	6.10
Rotor outer diameter (in.)	6.04
Stator stack length (in.)	3.40
End-turn length (in.)	0.88
Total axial length (in.)	5.16
Tooth thickness (in.)	0.38
Back-iron thickness (in.)	0.39
Magnet thickness (in.)	0.165
Minimum bridge thickness (in.)	0.04
Number of pole pairs	6
Slots per pole	3
Winding turns	3
Winding fill factor (%)	74

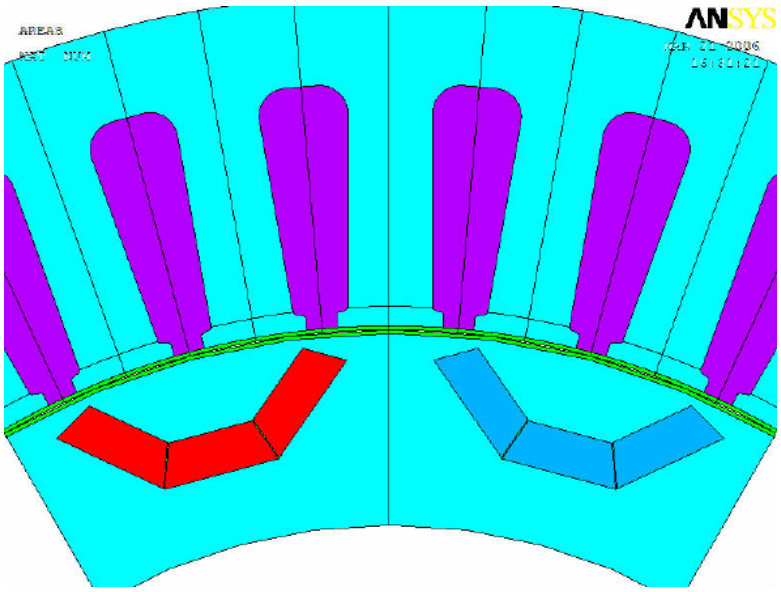

Fig. 3: UQM final motor design

Using the *most* conservative calculation described by UQM, the volume is 5.0 liters and the power-to-volume ratio is 10.9 kW/liter, a little short of the minimum 12.5 kW/liter requirement. But with the *least* conservative calculation using only these active materials, the volume falls to 3.8 liters and the power-to-volume rises to 14.6 kW/liter. Furthermore, the allowance of 0.88 in. made for each end-turn length seems much too large given that these should be "short-turn" coils wound directly around each tooth – this could be as little as 0.22 in., which yields 3.7 liters and 14.7 kW/liter with the *most* conservative calculation.

The UQM winding uses 24 AWG inverter grade magnet wire, formed as a multi-filament winding as three turns per pole, twelve coils per phase. The phase resistance is calculated using slot dimensions and fill factor to be 0.0067Ω, which rises to 0.0102Ω at a temperature of 150°C – the level assumed in the UQM report to allow for a reasonable temperature rise considering the 105°C ambient that is specified. However, under extreme steady state conditions, UQM also calculates that the rotor temperature could rise to about 160°C as shown in Figure 4 (UQM Figure 61). This means that the permanent magnets must be assumed to have stabilized after reaching this temperature.

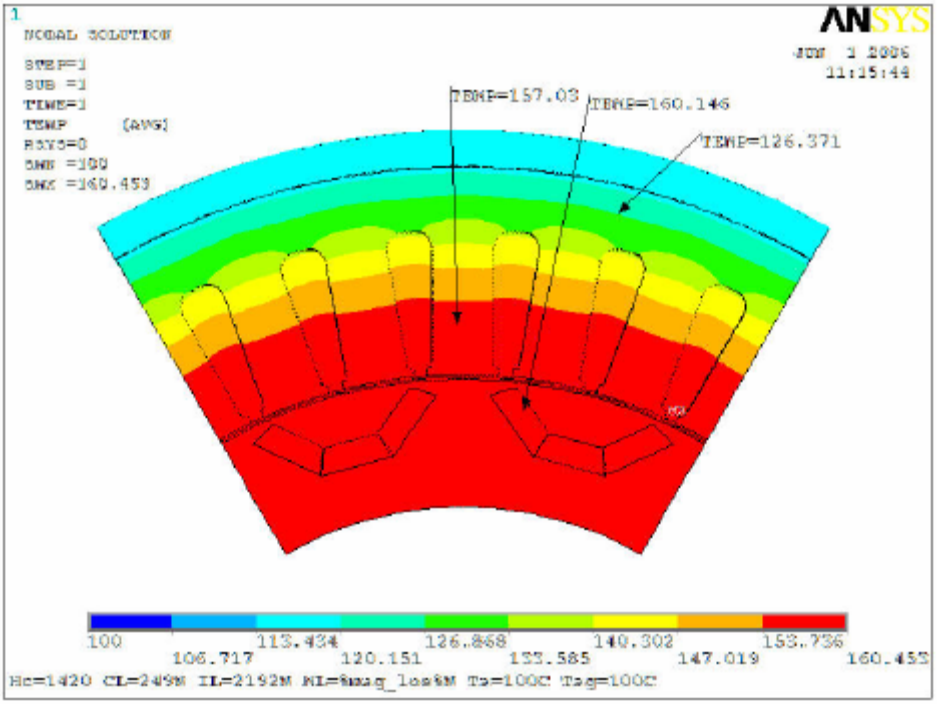

Fig. 4: UQM final design thermal analysis

The final design of the UQM motor is said to employ sintered neodymium-iron-boron (NdFeB) magnets with a remanence (B_r) of 11,000 Gauss at an operating temperature of 20°C. This suggests the actual use of an "N30UH" grade of NdFeB whose nominal B_r is 11,300 Gauss. The magnetic characteristics of this material (Figure 5) show a sufficiently high intrinsic coercivity (H_{ci}) to provide linear demagnetization throughout their second quadrant up to almost 180°C.

This is a simple method to demonstrate that the magnet should retain its fully magnetized state over its predicted operating temperature range.

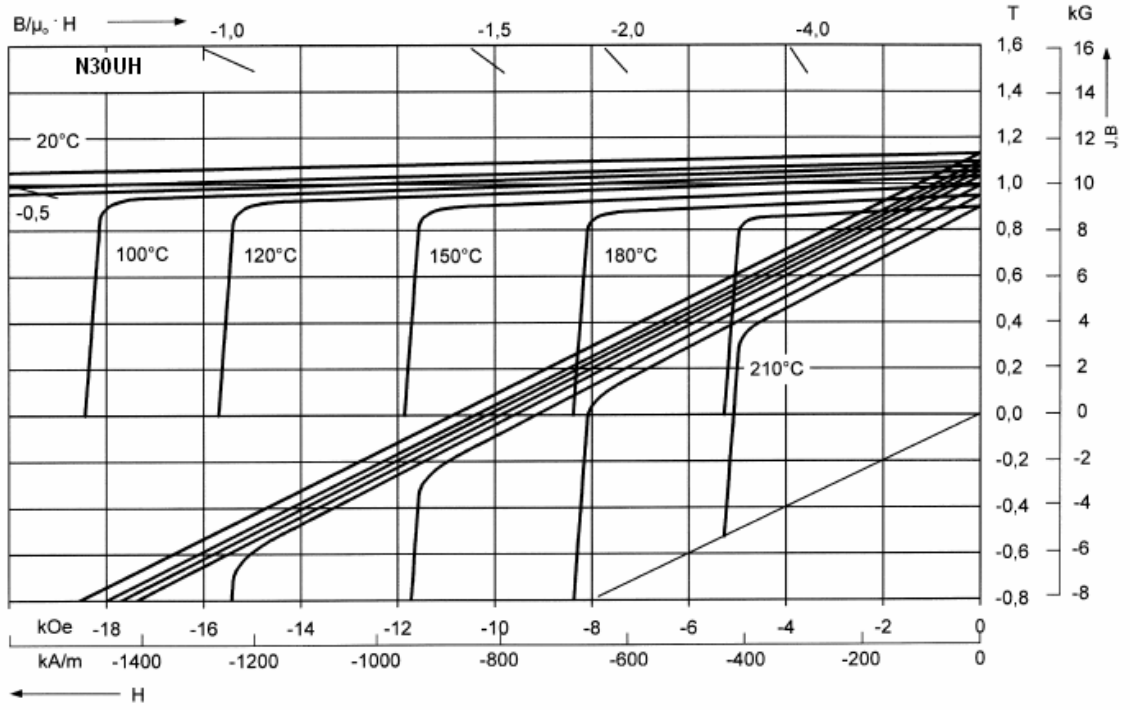

Fig. 5: Demagnetization characteristics of N30UH grade NdFeB

As temperature rises, the magnetic parameters of NdFeB fall below their room temperature levels and B_r declines at the rate α, the *"reversible temperature coefficient of B_r"*. For N30UH grade, α is –0.095%/^oC and B_r is reduced to 9,800 Gauss at 160^oC — this is the value that should have been be used to model the magnet in the UQM motor design, as the worst case assumption is that this component has not recovered from its worst case temperature excursion.

The UQM motor is designed to use non-oriented 29 gauge (0.014 in. thick) M19 electrical steel laminations, data on this specific grade and thickness material being available from a number of sources[3]. Iron losses can be computed at any speed and for any peak field (B) experienced at any place in the core using an expression of the form:

$$\text{Core loss (W/lb)} = (a+cB+eB^2+gB^3+iB^4+kB^5)/(1+bB+dB^2+fB^3+hB^4+jB^5),$$

where a through k are known constants. The magnetization characteristic of M19 steel is shown in Figure 6.

[3] *Armco Silicon Steels*, Proto Laminations Inc., www.protolam.com, July 1997.

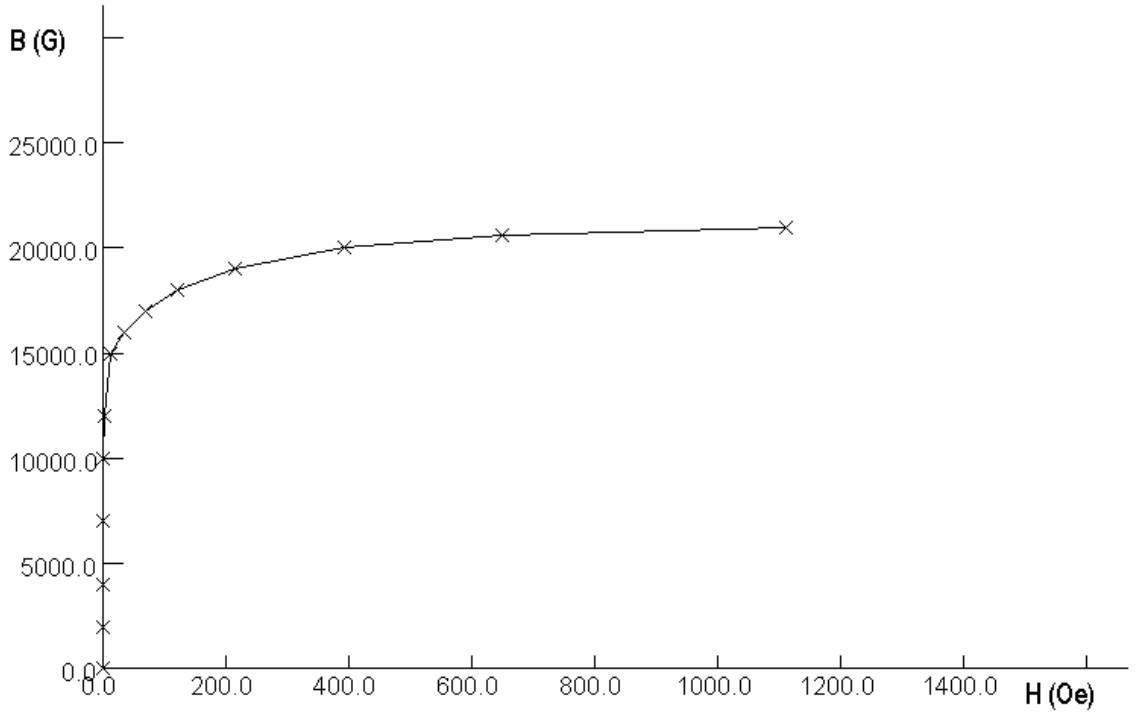

Fig. 6: Magnetization characteristic of M19 electrical steel

2.2: PHASOR DIAGRAM

The *interior permanent magnet* ("IPM") motor selected by UQM to meet the 2010 FreedomCAR specification is a hybrid between a traditional permanent magnet motor and a reluctance motor. The design of such a machine is quite well-known[4], and is characterized by the phasor diagram shown in Figure 7.

Voltages and torque are derived in the classical texts using d, q-axis theory, and from this phasor diagram (neglecting resistance R):

$$\omega\Psi_d = E_q + X_d I_d$$

The angular frequency (ω) is equal to p times the motor's angular velocity ω_m, where p is the number of pole pairs. The reluctance effect yields an additional q-component of flux linkage:

$$\omega\Psi_q = X_q I_q$$

Considering energy conversion in the rotor (and adding for three phases):

$$\omega_m T = 3\{\omega\Psi_d . I_q - \omega\Psi_q . I_d\}$$
$$= 3\{E_q I_q + (X_d - X_q) I_d I_q\}$$

[4] T.J.E. Miller, *Brushless Permanent-Magnet and Reluctance Motor Drives*, 1989, ISBN 0-19-859369-4, Oxford: Clarendon Press

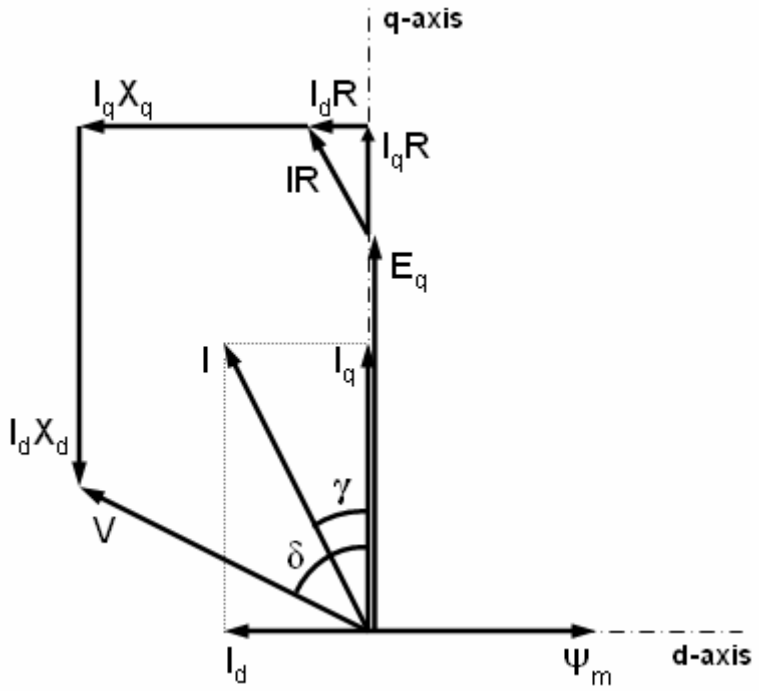

Fig. 7: Phasor diagram for a permanent magnet/reluctance hybrid motor

Quantities used in the phasor diagram are r.m.s. values, so the fundamental open circuit flux linkage (Ψ_m) due to the permanent magnet system alone is $1/\sqrt{2}$ times its peak flux linkage $N_{ph}\Phi_m$, where N_{ph} is the number of series turns per phase and Φ_m is the fundamental open circuit flux per pole. On open circuit, E_q is produced by Ψ_m, which is computed from the motor design. Likewise, d- and q-axis inductances are computed, and can be used in place of the reactances in the expression for torque:

$$T = 3p \{\Psi_m I_q – (L_q – L_d)I_d I_q\}$$

This equation is valid even if resistance is not zero. Its first term is the *alignment* torque due to the magnet and the second term is the *reluctance* torque due to saliency in the rotor's magnetic circuit, which relies upon $L_q > L_d$ (note that I_d is normally negative). In a "surface-magnet" type of motor there is no saliency and no reluctance torque since $L_d = L_q$, so torque becomes the familiar expression:

$$T = 3p\Psi_m I_q = (3p/\omega).E_q I_q$$

2.3: UQM FINAL DESIGN MODEL

The performance of the benchmark UQM final motor and the subsequent variants on this design were evaluated using the finite element analysis ("FEA") program "Opera" developed by Vector Fields Ltd. The dimensions for the UQM design given in Table 3 and Figure 3 were replicated into "Opera" for axi-symmetric solution as shown in Figure 8, where regions 2 through 4 are the N30UH grade NdFeB permanent magnets with edges beveled as prescribed by

UQM, regions 6 and 13 are M19 electrical steel laminations, and regions 1 and 8 through 12 are sides of each winding coil (grey colored regions are non-magnetic).

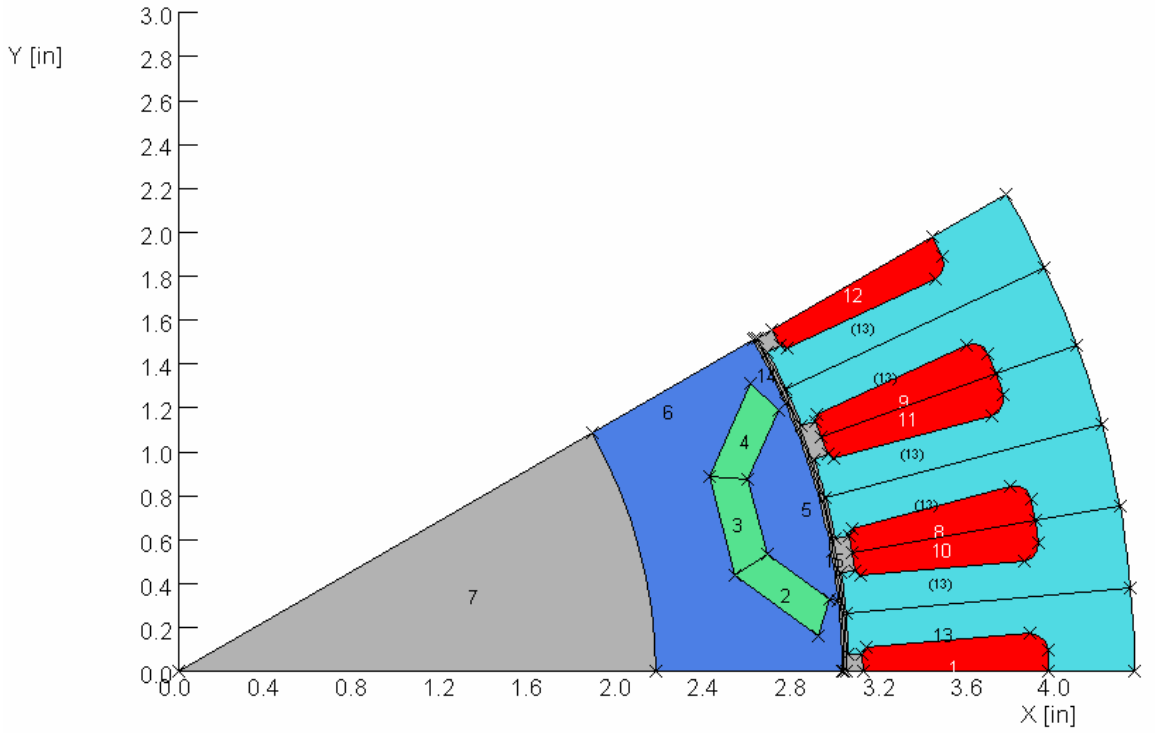

Fig. 8: Layout of final UQM motor design in "Opera" FEA program

The maximum allowable current according to the specification given in Table 1 is 400A, which with 3 turns/pole is equivalent to 1200 Ampère-turns in a coil. The peak demagnetization of the magnets occurs when this excitation is applied directly towards them along the d-axes, i.e. when γ (Figure 7) approaches 90°. The corresponding FEA in Figure 9 shows the flux density magnitude distribution using the 160°C magnet B_r of 9,800 Gauss (called "BMOD" in "Opera", with units in Gauss). This applied field almost completely excludes magnet flux from the stator, concentrating it instead around the magnets and through the bridges in the rotor structure. Figure 9 also illustrates that flux density is fairly uniform throughout the magnet, with a demagnetizing field close to –4000 Oe which is safely above the 160°C coercivity of –9400 Oe.

The peak operating profile in Figure 1 showed the torque that the motor is required to develop at the minimum 200V supply voltage and with a maximum allowable phase current of 400A. Allowing for a 10V d.c. voltage drop in the inverter, the r.m.s. voltage per phase which corresponds to 200V d.c. supply is 77.6V. Calculation of motor performance via the phasor diagram of the previous section requires values for Ψ_m, L_d and L_q, all of which may be determined using

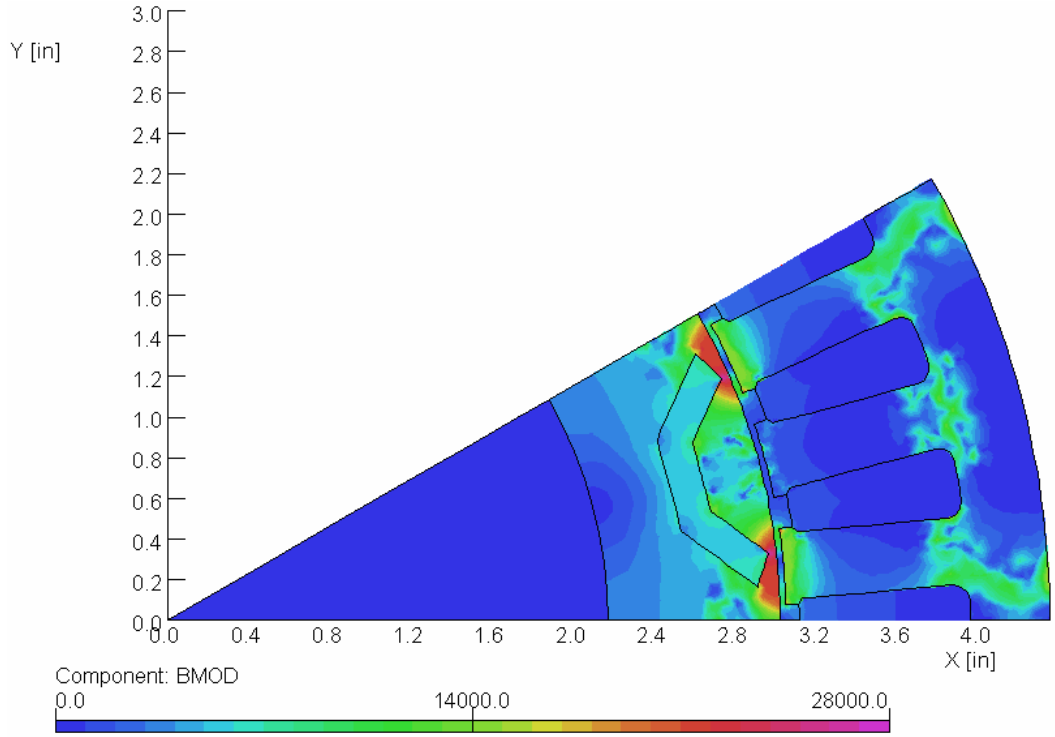

Fig. 9: Flux density in final UQM motor design at peak demagnetization

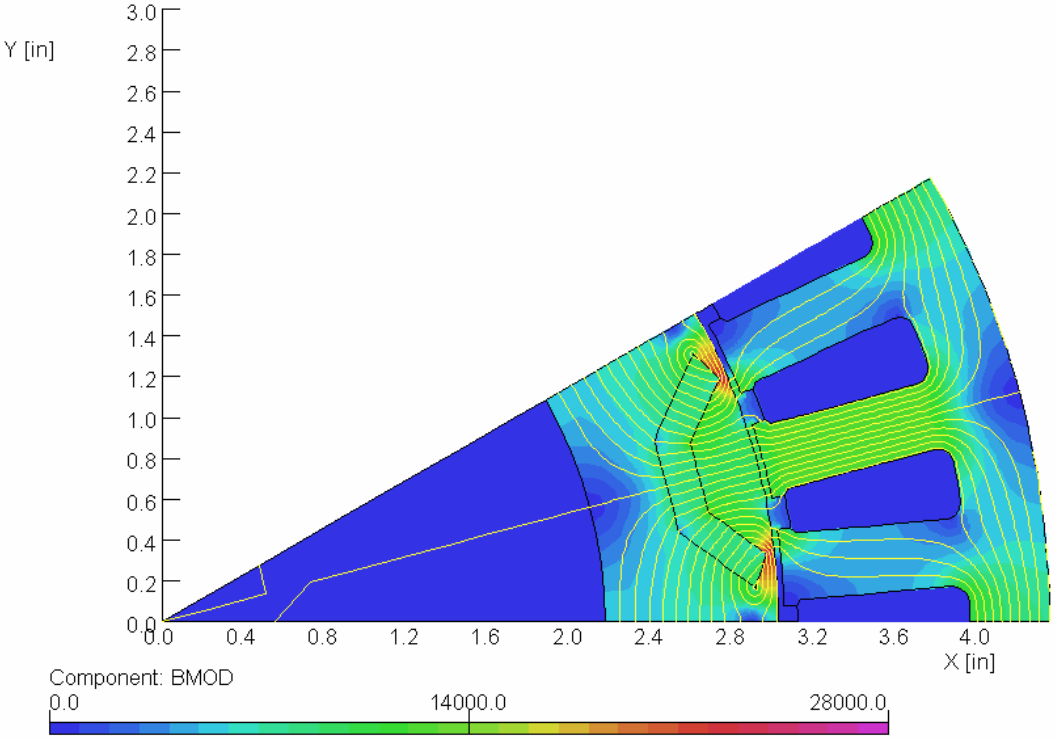

Fig. 10: Open circuit flux distribution in final UQM motor design

FEA. As its description suggests, the fundamental open circuit flux linkage (Ψ_m) due to the permanent magnet system alone is calculated from the FEA solution without excitation currents in Figure 10 — in this case, Ψ_m per pole = 0.037 Wb.

Because of non-linearity in the core material (Figure 6), both L_d and L_q will be functions of the excitation level, i.e. of the magnitude and phase (I, γ) of current required to produce the required torque at a given speed. An iterative solution is therefore required at each operating point to find consistent values for L_d, L_q, I_d and I_q. By evaluating flux linkages on the d- and q-axes using FEA, inductances may be calculated using:

$$\Psi_d = L_d I_d + \Psi_m \; ; \quad \Psi_q = L_q I_q$$

I and γ are then adjusted and the flux linkages re-computed until convergence of the solution is achieved. An example solution that was used to find Ψ_q is shown in Figure 11.

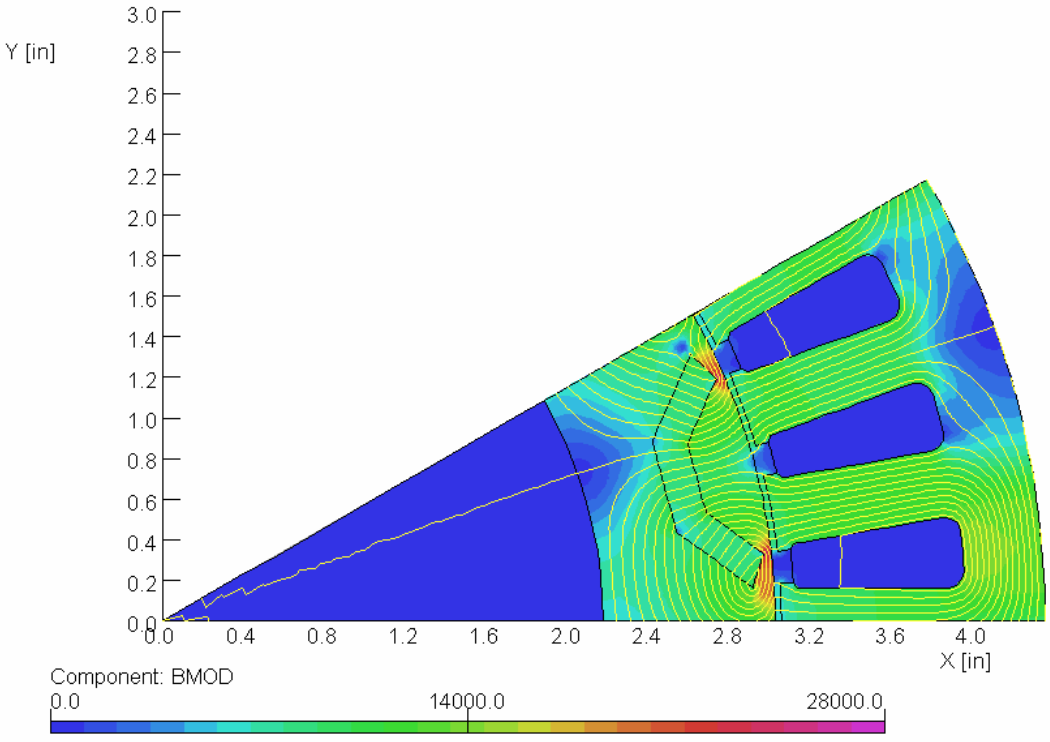

Fig. 11: Example q-axis flux distribution in final UQM motor design

Because of the procedure adopted for this iterative solution, L_d and L_q were only evaluated at the required values of I_d and I_q, so these are shown in Figure 12 over somewhat different ranges. These variations are of a similar form to those presented in the UQM report, except that L_q shown here is somewhat higher, particularly at low current. The q-axis inductance is influenced more strongly by the core material while the d-axis is dominated by the permanent magnets, so a

more accurate magnetization characteristic for M19 electrical steel at low fields as in Figure 6 can easily account for this difference.

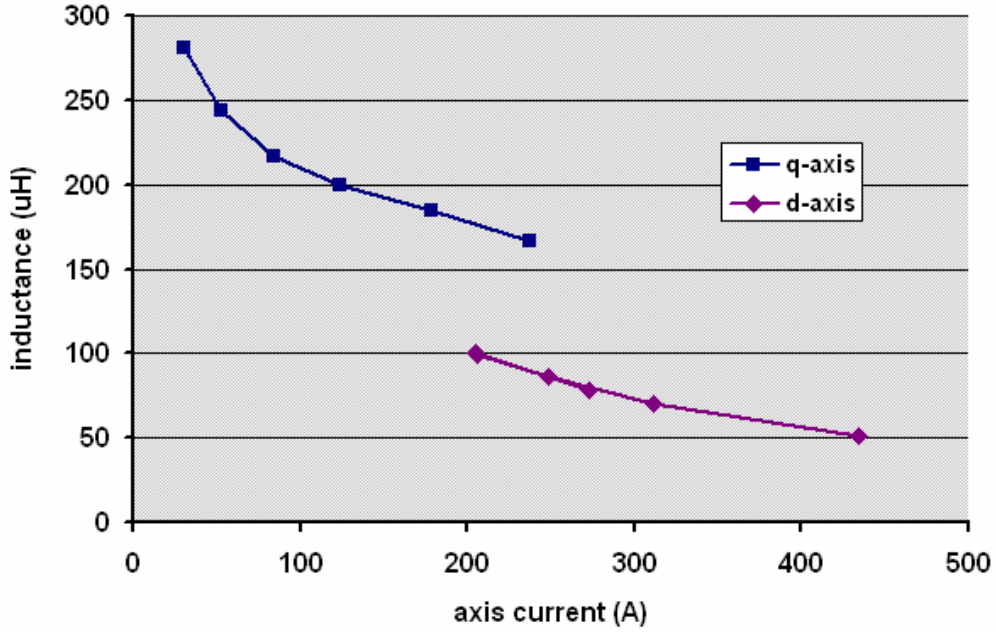

Fig. 12: Inductance vs. current in final UQM motor design

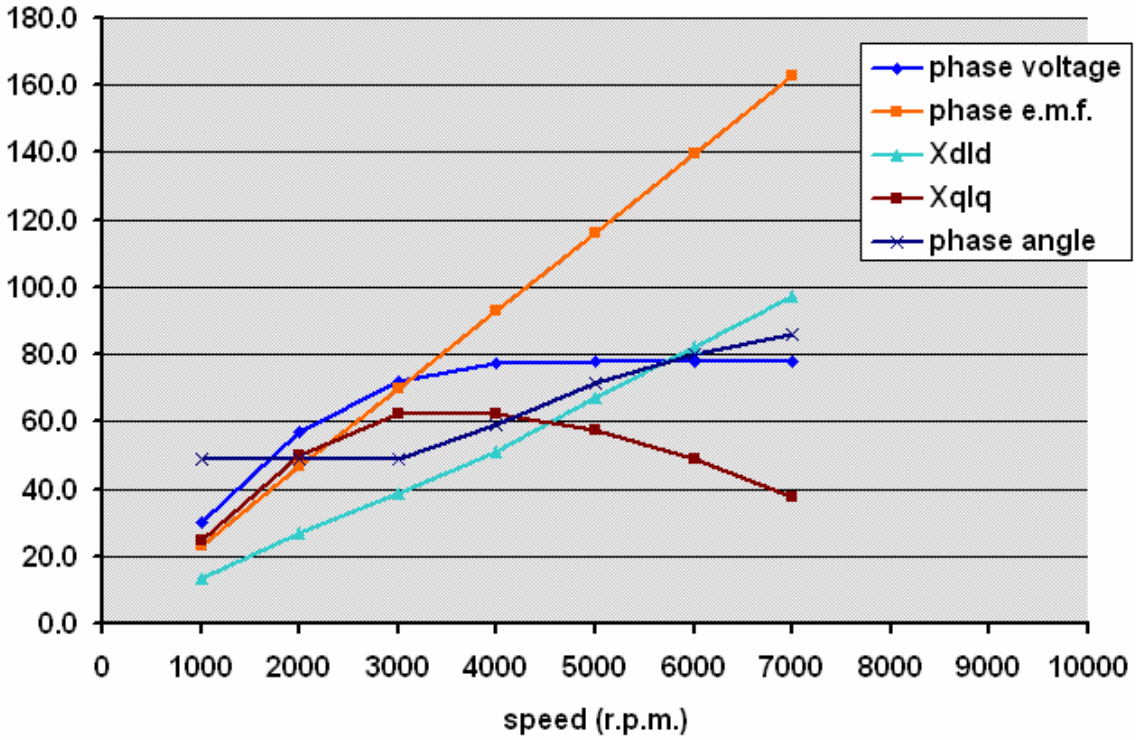

Fig. 13: Phasor quantities at 200V d.c. for the final UQM motor design

The phasor quantities calculated in this study are shown in Figure 13, the transitions in each curve (except for phase angle) being relatively smooth; this is in contrast to those presented in the UQM report (its Figure 50), particularly its calculation of $X_d I_d$. Capping of the voltage at 77.6V r.m.s., equivalent to the 200V d.c. minimum supply voltage, is achieved by advancing the phase angle γ from an initial 49^o towards 86^o at 7,000 rev/min. At this and higher speeds as shown in Figure 14, the allowable phase current of 400A has been exceeded, and this design is no longer viable.

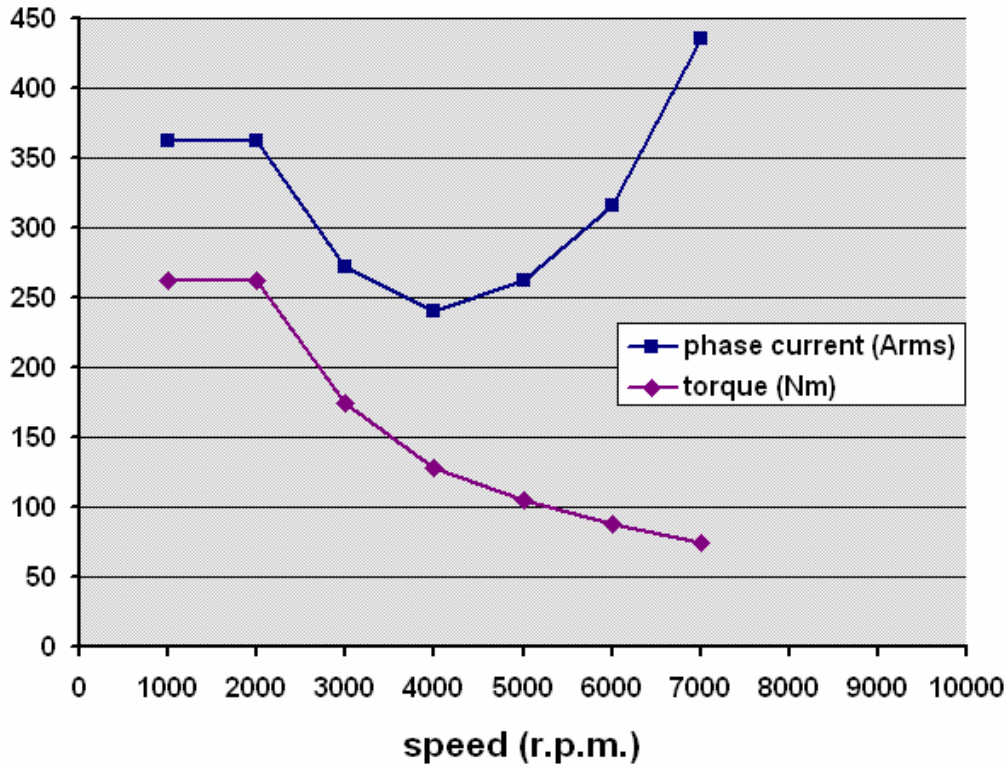

Fig. 14: Current profile at 200V d.c. for the final UQM motor design

In a similar fashion to the discrepancy noted for L_q, the phase back-e.m.f. E_q is somewhat higher than that presented in the UQM report (its Figure 50), and this provides a suggestion as to how this design might be adjusted in order to meet the required performance specification. Note that open circuit flux linkage (Ψ_m) due to the permanent magnet system alone is equal to E_q/ω, so the field provided by the magnets into this magnetic circuit may in fact be slightly too strong. The effect of this might be to prevent this machine from functioning properly as a hybrid between a permanent magnet motor and a reluctance motor, in which the constant power feature of the peak operating profile (Figure 1) must be achieved by field weakening. The correction for this discrepancy will be discussed later.

3: MOTORS USING COMMERCIAL NdFeB MAGNETS

3.1: ANISOTROPIC SINTERED NdFeB

The *remanence* B_r and *intrinsic coercivity* H_{ci} of all types of commercially available NdFeB magnets are plotted in Figure 15, encompassing those made by all of the most common processes. This illustrates quite clearly the significant performance advantage that anisotropic sintered NdFeB offers over anisotropic ceramic ferrite, followed closely by anisotropic bonded NdFeB.

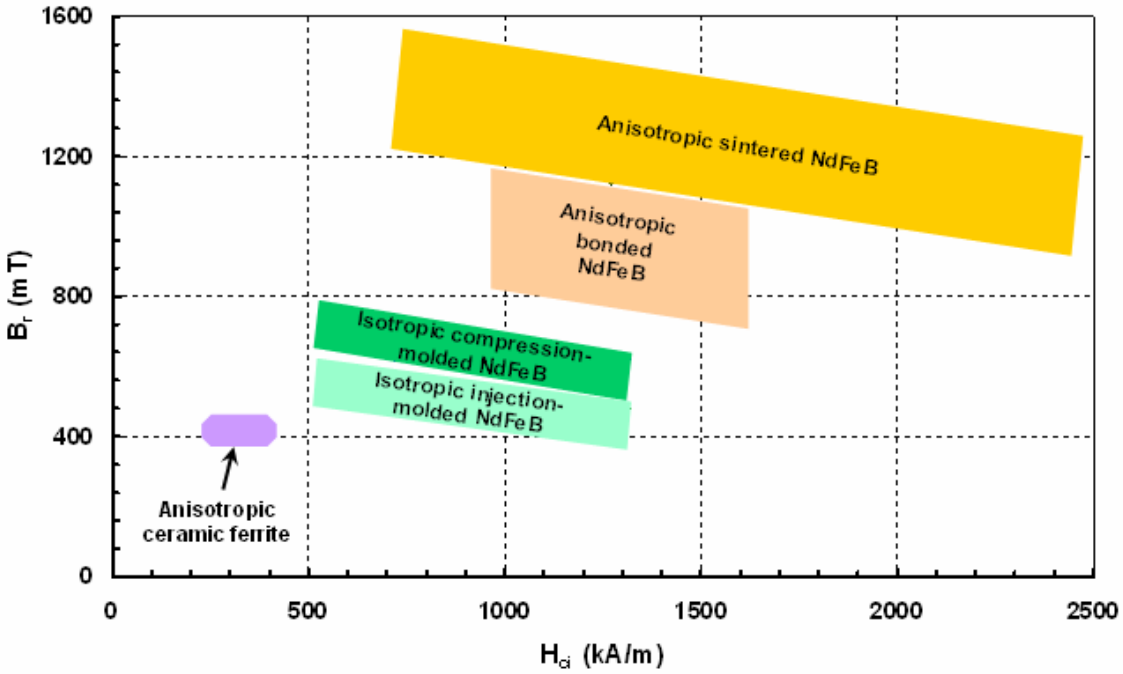

Fig. 15: Magnetic property overview of NdFeB magnets

In simple shapes such as the rectangular blocks proposed for this IPM motor, the most economical source for sintered NdFeB is from China, a leading licensed supplier being Beijing Zhong Ke San Huan High-Tech Co., Ltd. ("San Huan"). The names used by San Huan for their sintered NdFeB grades closely follow today's industry standards, the properties for which are summarized in Table 4. Maximum operating temperature is deduced from linearity of the second quadrant demagnetization characteristics, which is closely linked to the magnitude of H_{ci} as is evident from this table. Only the "UH" and "EH" grades are suitable for the required operation at 160°C, and while the composition of "EH" provides higher H_{ci} than "UH" grades, it does so with reduced B_r. As we have seen, "UH" is a suitable grade choice if sintered NdFeB is to be used in this IPM motor, and we will not want to accept a lower B_r than that offered by the N30UH material that has already been selected.

Table 4: Properties of commercial San Huan sintered NdFeB magnets

Grade	Remanence B_r		Coercivity H_c		Intrinsic Coercivity H_{ci}		$(BH)_{max}$		Curie Temp. T_C	Maximum Operating Temp.
	T	kG	kA/m	kOe	kA/m	KOe	kJ/m^3	MGOe	°C	°C
N-30	1.08-1.15	10.8-11.5	780-836	9.8-10.5	>955	>12	220-240	28-31	310	80-100
N-33	1.13-1.17	11.3-11.7	795-880	10.0-11.1	>955	>12	245-260	31-33	310	80-100
N-35	1.18-1.22	11.8-12.2	875-915	11.0-11.5	>955	>12	260-285	33-36	310	80-100
N-38	1.22-1.26	12.2-12.6	860-915	10.8-11.5	>955	>12	285-303	36-38	310	80-100
N-40	1.26-1.29	12.6-12.9	836-876	10.5-11.0	>955	>12	303-318	38-40	310	80-100
N-42	1.29-1.33	12.9-13.3	836-876	10.5-11.5	>955	>12	318-342	40-42	310	80-100
N-45	1.33-1.37	13.3-13.7	836-876	10.5-11.0	>955	>12	342-358	42-45	310	80-100
N-48	1.37-1.43	13.7-14.3	916-1114	11.5-14.0	>955	>12	358-364	46-49	310	80-100
N-27H	1.02-1.10	10.2-11.0	765-835	9.6-10.5	>1353	>17	195-220	25-28	340	120
N-30H	1.08-1.15	10.8-11.5	810-850	10.2-10.7	>1353	>17	220-245	28-31	340	120
N-33H	1.14-1.17	11.4-11.7	820-876	10.3-11.0	>1353	>17	247-263	31-33	340	120
N-35H	1.17-1.21	11.7-12.1	860-915	10.8-11.5	>1353	>17	263-279	33-35	340	120
N-38H	1.22-1.26	12.2-12.6	915-955	11.5-12.0	>1353	>17	287-303	36-38	340	120
N-40H	1.26-1.29	12.6-12.9	915-955	11.5-12.0	>1353	>17	303-318	38-40	340	120
N-27SH	1.02-1.10	10.2-11.0	765-835	9.6-10.5	>1595	>20	195-220	25-28	350	150
N-30SH	1.08-1.12	10.8-11.2	812-852	10.2-10.7	>1595	>20	216-246	27-30	350	150
N-33SH	1.14-1.17	11.4-11.7	740-876	10.3-11.0	>1595	>20	247-263	31-33	350	150
N-35SH	1.17-1.21	11.7-12.1	860-915	10.8-11.0	>1595	>20	263-279	33-35	350	150
N-25UH	0.98-1.02	9.8-10.2	732-764	9.2-9.6	>1990	>25	183-199	23-25	350	180
N-28UH	1.04-1.08	10.4-10.8	780-812	9.8-10.8	>1990	>25	183-223	23-25	350	180
N-30UH	1.08-1.12	10.8-11.2	804-844	10.1-10.6	>1990	>25	223-239	28-30	350	180
N-33UH	1.14-1.17	11.4-11.7	740-876	10.3-11.0	>1990	>25	247-263	31-33	350	180
N-25EH	0.98-1.02	9.8-10.2	732-764	9.2-9.6	>2387	>30	183-199	23-25	350	200
N-28EH	1.04-1.08	10.4-10.8	780-812	9.8-10.2	>2387	>30	207-223	26-28	350	200

3.2: IPM MOTOR DESIGN WITH SINTERED NdFeB

In the foregoing analysis it was found that the final UQM motor design may not function properly as a hybrid between a permanent magnet motor and a reluctance motor because the field provided by the magnets into its magnetic circuit may in fact be slightly too strong. After several modifications to the UQM motor layout were tried, it was found that reduction in magnet thickness from 0.165" to 0.100" would provide the required performance over the full operating speed range. This simple change is evident in Figure16 in comparison to the original layout from Figure 8.

Because the chosen N30UH grade of sintered NdFeB magnet already has a significantly high H_{ci}, we find that this is sufficient to prevent irreversible demagnetization even with the reduced magnet thickness. With the maximum allowable excitation of 1200 Ampère-turns in a coil applied directly towards the magnets along the d-axes (when γ approaches 90^o), the corresponding FEA in Figure 17 shows the flux density magnitude distribution using the 160^oC magnet B_r of 9,800 Gauss. This again illustrates that flux density is fairly uniform throughout the magnet, with a demagnetizing field close to –5600 Oe. As expected, this has increased from the -4000 Oe level calculated with the original thicker magnets, but is still safely above the 160^oC coercivity of –9400 Oe.

The fundamental open circuit flux linkage due to the permanent magnet system alone is calculated from the FEA solution without excitation currents in Figure 18 to be Ψ_m per pole = 0.032 Wb, reduced as expected from the original 0.037 Wb.

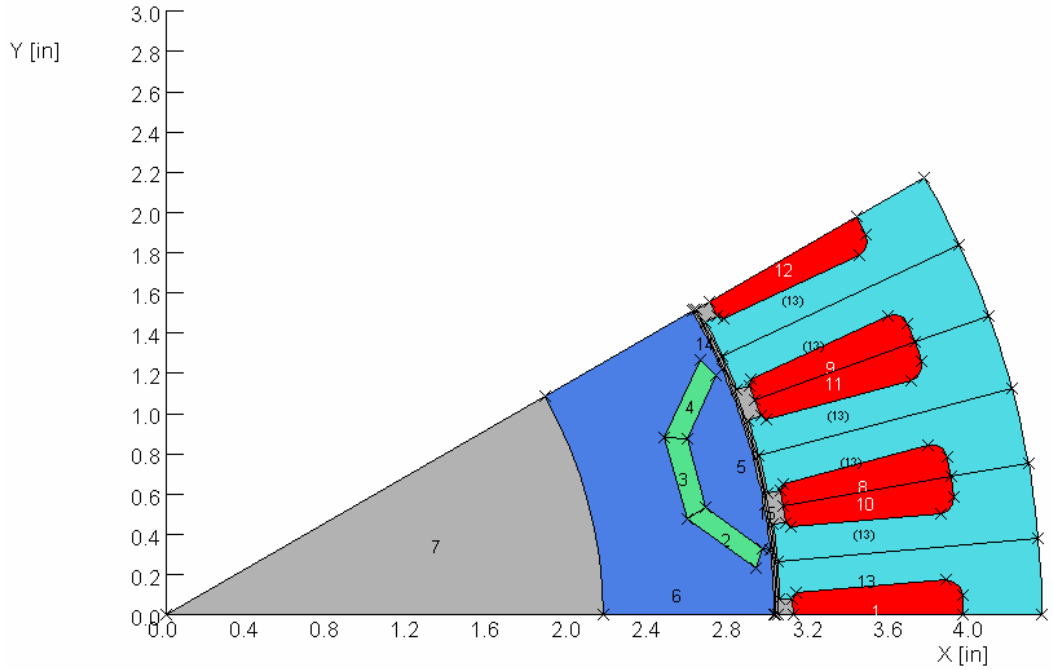

Fig. 16: Layout of modified UQM motor design in "Opera" FEA program

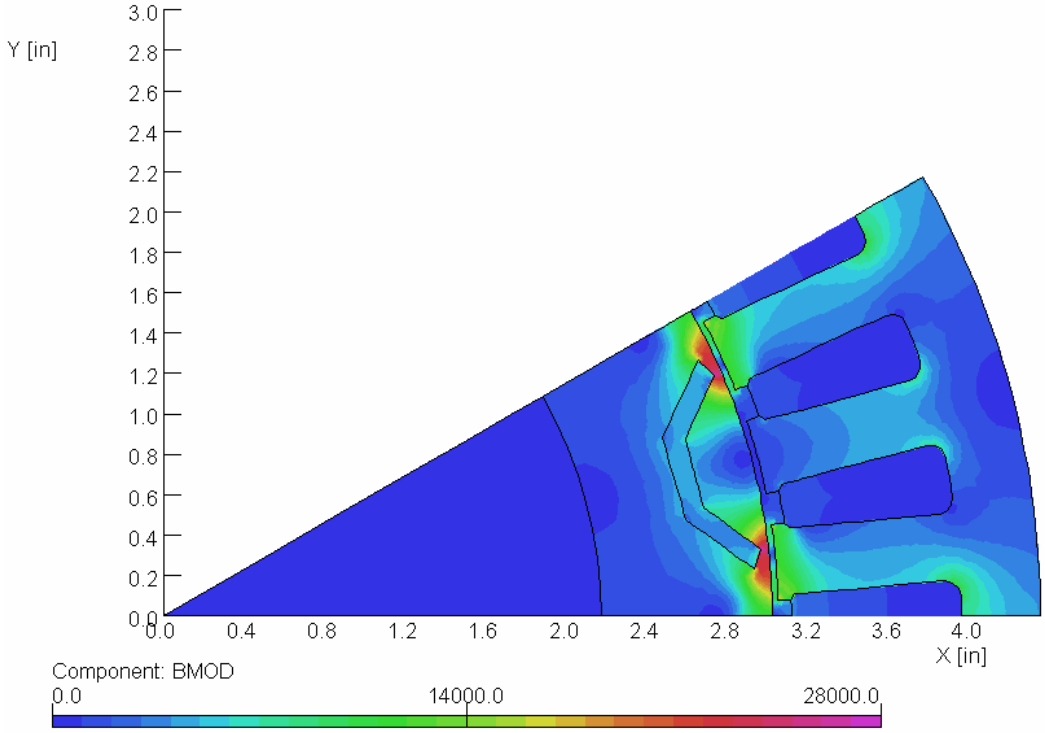

Fig. 17: Flux density in modified UQM motor design at peak demagnetization

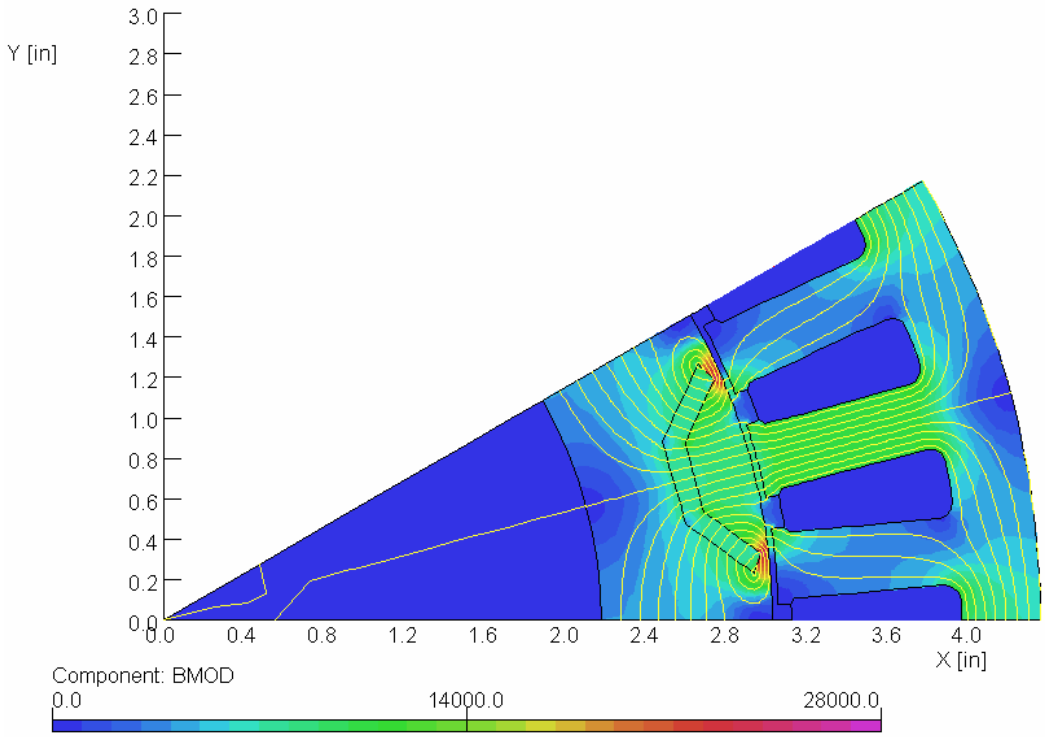

Fig. 18: Open circuit flux distribution in modified UQM motor design

As described in Section 2.3, an iterative solution is employed using FEA in which I and γ are adjusted and the flux linkages re-computed until convergence is achieved. The inductances L_d and L_q were only evaluated at the required values of I_d and I_q and thus over somewhat different ranges as shown in Figure 19. There is very little perceptible change in the variations of L_q with I_q and L_d with I_d compared to Figure 12 for the original UQM motor design, even though the magnets centered on the d-axes are slightly shorter now.

The phasor quantities calculated for the motor using the shorter magnets are shown in Figure 20, the transitions in each curve (except for phase angle) still being relatively smooth. Capping of the voltage at 77.6V r.m.s., equivalent to the 200V d.c. minimum supply voltage, is achieved by advancing the phase angle γ from an initial 40^o towards 86^o at 10,000 rev/min. There is a noticeable improvement in the q-axis component $X_q I_q$ compared to our calculations for the original UQM motor design in Figure 13, which collapsed at higher speeds but now holds up to provide reluctance torque up to full speed. And as shown in Figure 21, the motor is now able to achieve its required peak operating profile over the full speed range without exceeding the allowable phase current of 400A.

The operating profile for efficiency shown in Figure 2 described the further requirement for efficiency to exceed 93% at 20% of rated torque (i.e. 52 Nm) at speeds ranging from 1,000 to 10,000 rev/min. Unlike the peak operating profile,

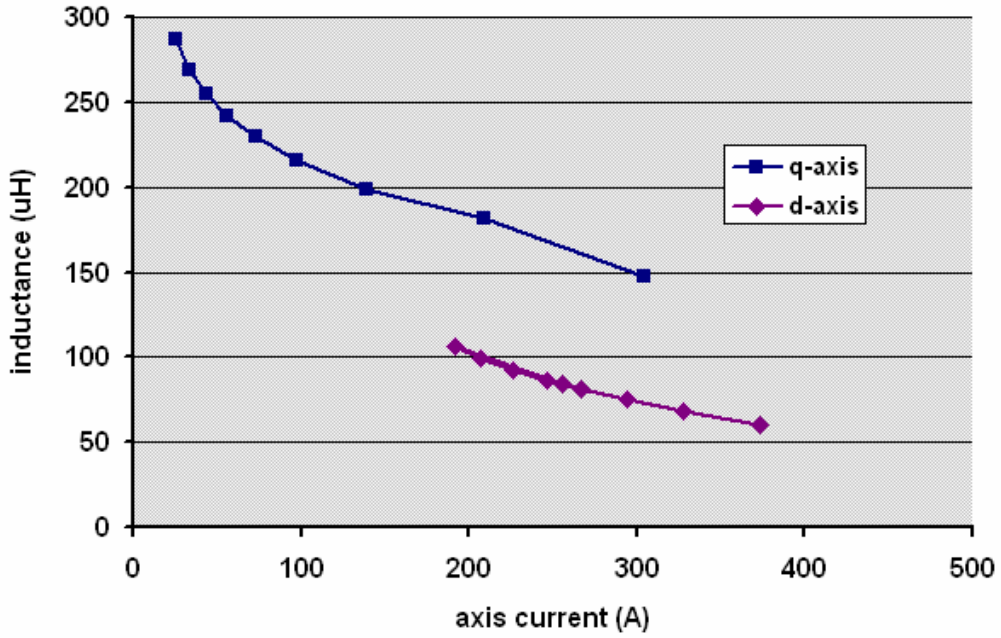

Fig. 19: Inductance vs. current in modified UQM motor design

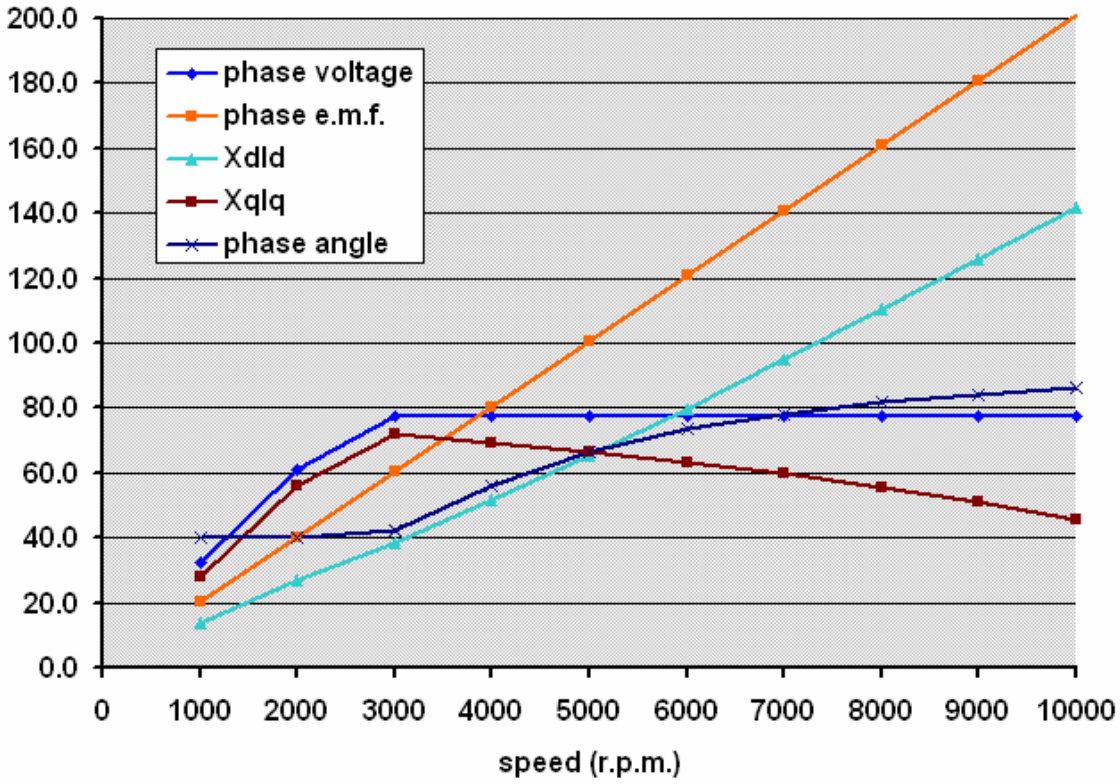

Fig. 20: Phasor quantities at 200V d.c. for modified UQM motor design

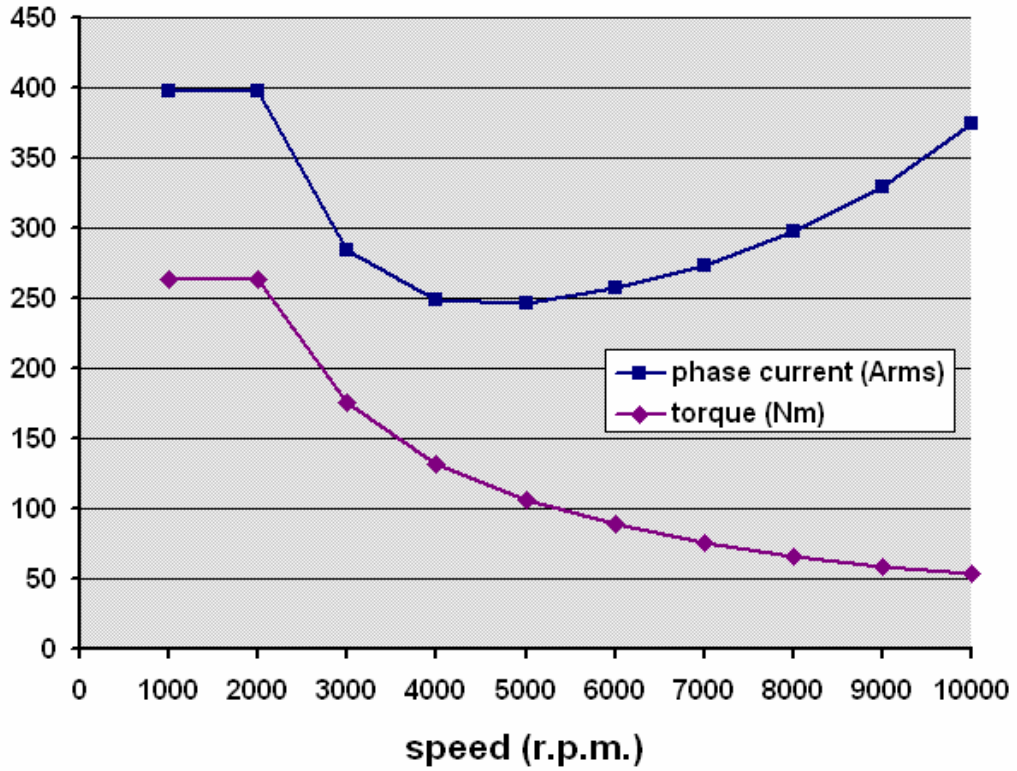

Fig. 21: Current profile at 200V d.c. for modified UQM motor design

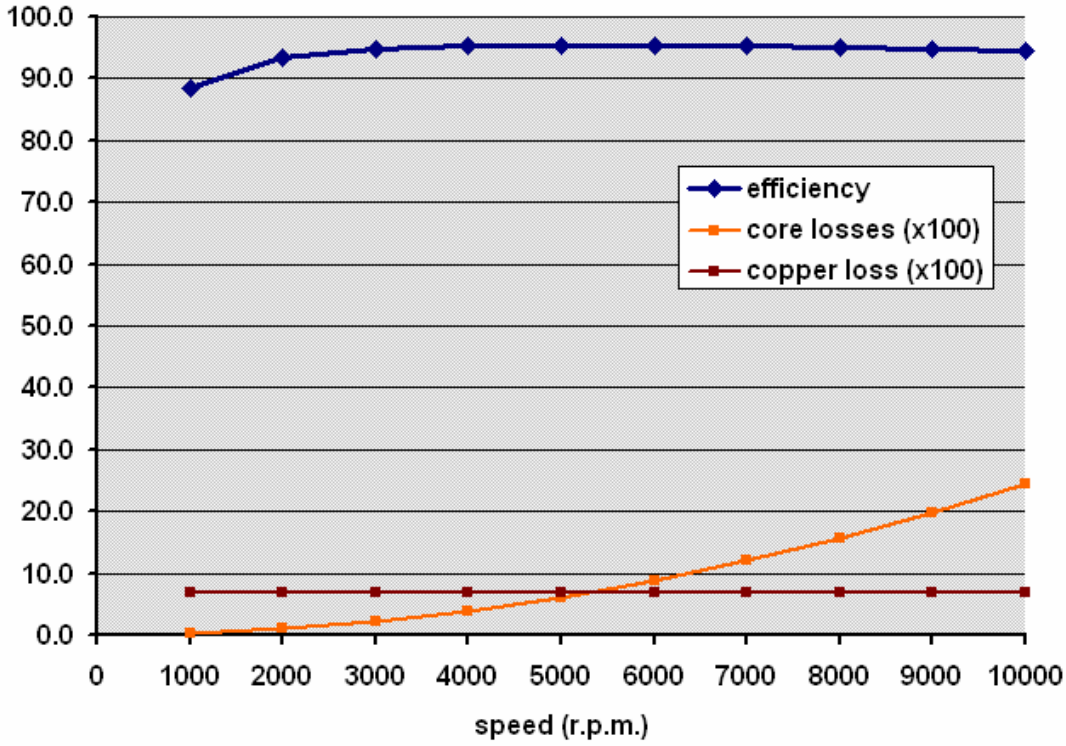

Fig. 22: Efficiency at 325V d.c. for modified UQM motor design (20% torque, 52 Nm)

this efficiency is to be calculated at the nominal 325V supply voltage. Allowing for a 10V d.c. voltage drop in the inverter, the r.m.s. voltage per phase which corresponds to 325V d.c. supply is 128.6V. In this modified UQM motor design, 52 Nm is achieved over the entire 1,000 to 10,000 rev/min range with a constant phase angle γ of 64.5^{o} and hence a constant phase current of 150A. This means that the I^2R power loss in the winding will be constant over this speed range, although the core losses in the magnetic circuit will vary because they are a function of both the peak field distribution (B) and the speed as discussed in Section 2.1. Figure 22 shows that the target efficiency of >93% is achieved from 2,000 to 10,000 rev/min, falling below this to 89% at 1,000 rev/min. A maximum efficiency of 95.5% is reached at about 5,000 rev/min and 52 Nm.

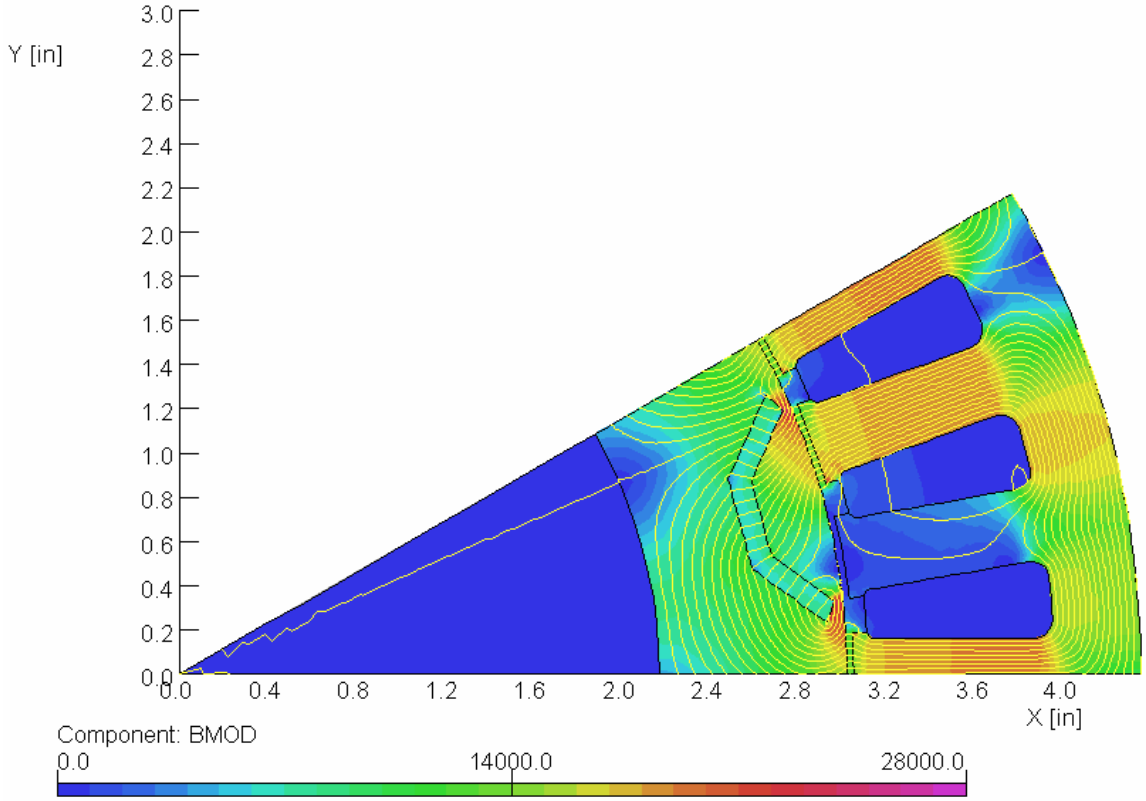

Fig. 23: Maximum electromagnetic stress in modified UQM motor design

It is clear from all the foregoing flux density plots that the greatest concentration of magnetic flux is at the narrow regions in the rotor that bridge the magnet slots with the rotor circumference. In the final UQM design this minimum bridge thickness has been specified as 0.040". Of concern is that the mechanical stress developed in these regions should affect the integrity of the rotor, so FEA is used to calculate the component of this stress which is due to electromagnetic forces developed in the magnetic circuit. With the maximum allowable phase current applied to the winding, the phase angle γ is varied until the maximum electromagnetic component of stress is found in the position shown in Figure 23.

The corresponding flux density distribution along this 30° pole pitch section of the rotor surface is shown in Figure 24. Across the 0.040" bridge section, this yields the component of stress due to electromagnetic forces of 6.35 MPa. However, the other component due to centrifugal force on the rotor is much greater than this. Calculated from the geometry of the rotor section above the magnet slots, the component of stress due to centrifugal force at 10,000 rev/min is 112.60 MPa, giving a total stress across the 0.040" bridge section of 118.95 MPa. This is safely within the 350 MPa yield strength of M19 electrical lamination steel.

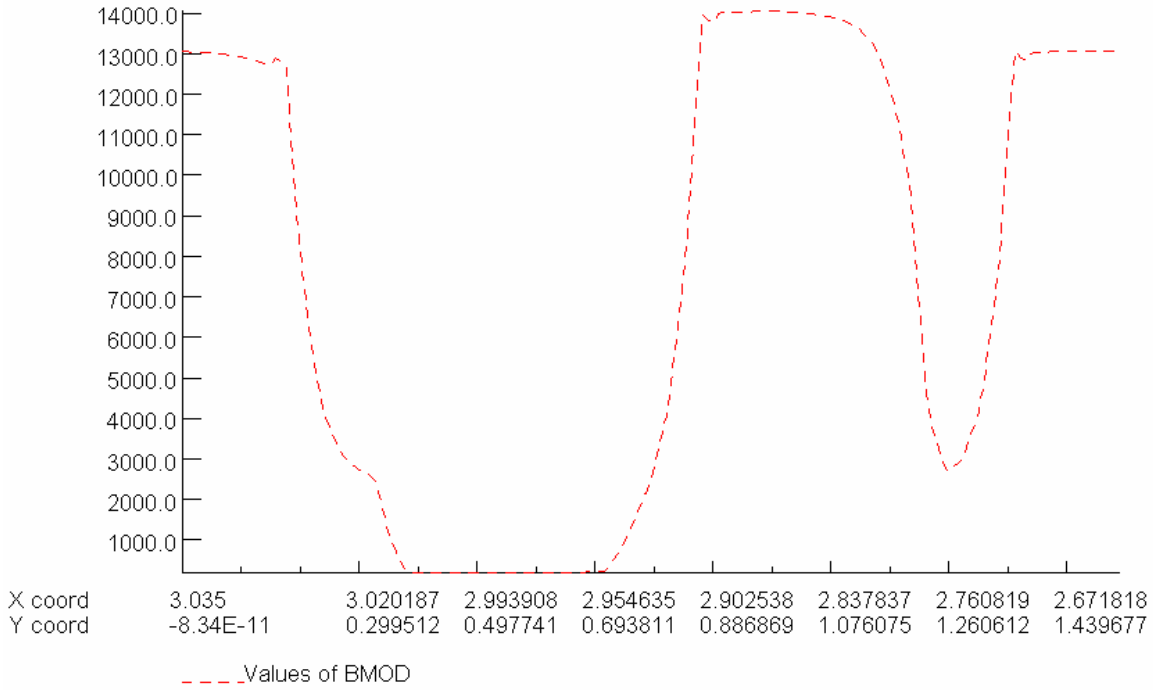

Fig. 24: Flux density distribution from one pole pitch for maximum electromagnetic stress in modified UQM motor design

3.3: ANISOTROPIC BONDED NdFeB

While isotropic bonded NdFeB magnets are well-known, anisotropic types have hardly found commercial application. The most common process to make stable powder for subsequent compounding and molding is by hydrogenation, disproportionation, desorption and recombination ("HDDR"). As its name suggests, this process involves the absorption of hydrogen, which gives the consequent material inherently poorer performance at elevated temperatures. Aichi Steel Corporation is perhaps the only company to have had any notable success in commercializing state-of-the-art HDDR NdFeB powder and anisotropic bonded magnets made from it. Its "MAGFINE" grade MF25 material is a suitable grade choice if anisotropic bonded NdFeB is to be used in this IPM motor, and we will not want to accept a lower B_r provided that its H_{ci} is sufficient to prevent demagnetization at high temperature. Its powder remanence of

13,800 Gauss translates to a B_r of 10,840 Gauss in a compression-molded magnet (Figure 25). MF25 has been shown[5] to operate satisfactorily up to 150°C in commercial applications, and can be stabilized somewhat higher than this as shown in Figure 26.

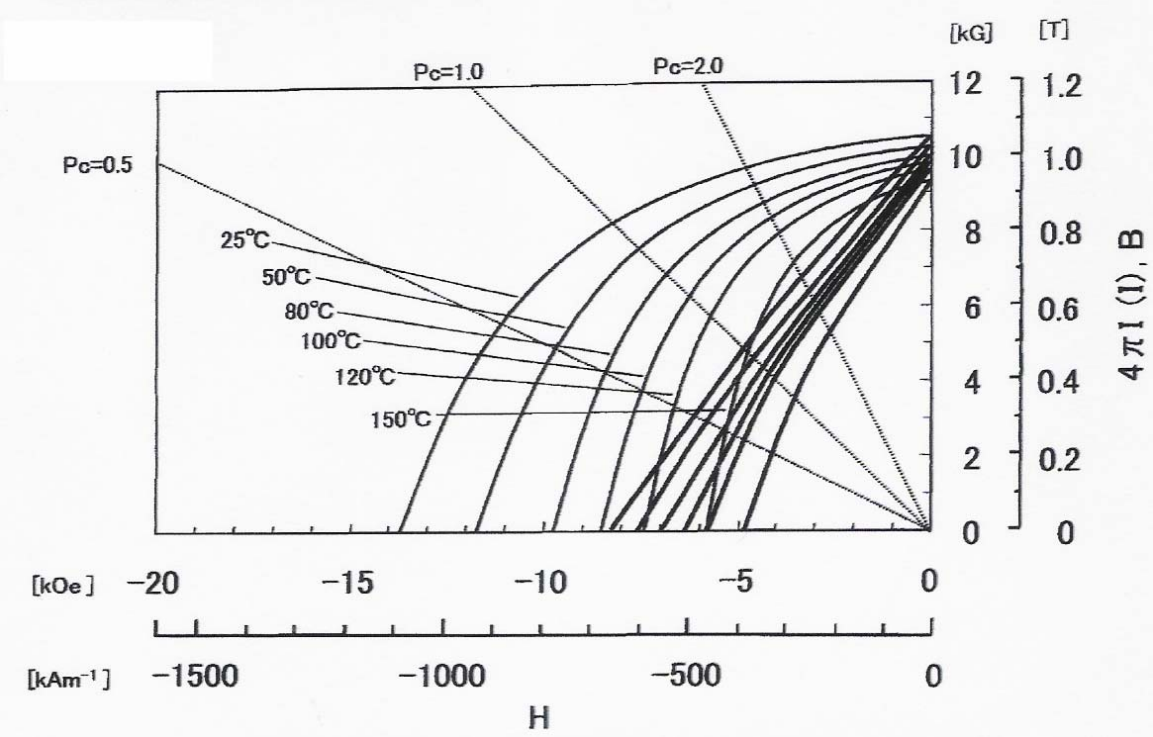

Fig. 25: Demagnetization characteristics of Aichi MF25 grade compression-molded NdFeB

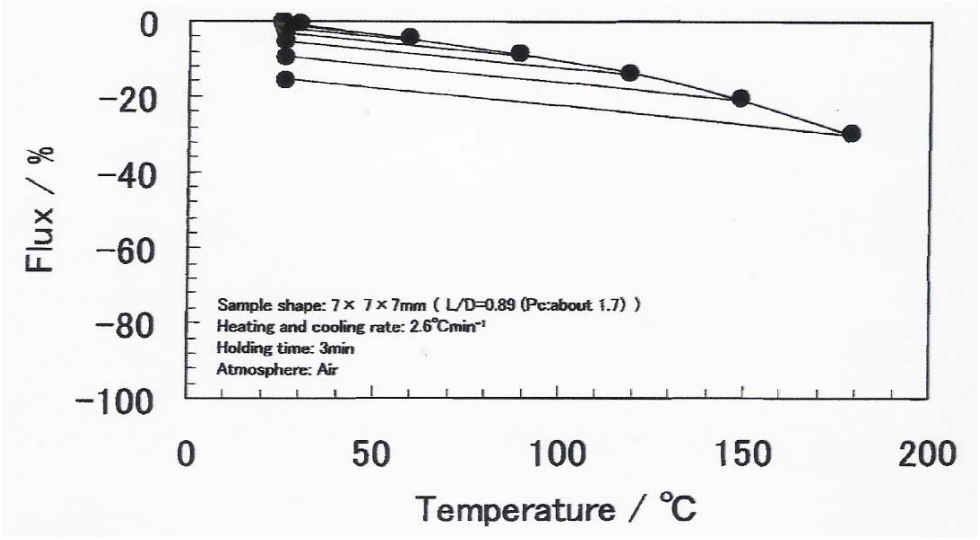

Fig. 26: Heat cycle characteristics of Aichi MF25 grade compression-molded NdFeB

[5] N. Hamada, K. Noguchi, C. Mishima and Y. Honkura, "Development of anisotropic bonded magnet applied to 150°C use", *I.E.E.E. Trans. Magn.*, vol. 41, pp. 3847-49, October 2005.

3.4: IPM MOTOR DESIGN WITH ANISOTROPIC BONDED NdFeB

Several iterations of the motor design were tried using compression-molded MF25 magnet material with a demagnetization characteristic at 160°C derived from Aichi data. It was found that a similar layout to the original UQM design would provide the required performance over the full operating speed range, but with a variable magnet thickness as shown in Figure 27. With the maximum allowable excitation of 1200 Ampère-turns in a coil applied directly towards the magnets along the d-axes (when γ approaches 90°), the corresponding FEA in Figure 28 shows the flux density magnitude distribution using the 160°C magnet B_r of 9,350 Gauss. The thickness profile for the magnets had been adjusted until a fairly uniform demagnetizing field of about –2800 Oe was obtained throughout all the magnets. For this condition, the center section of magnet (region 3) is 0.200" thick, and the side sections (regions 2 and 4) taper from 0.189" to 0.165" thick towards the outer ends. For the subsequent analysis of this motor's performance, it was therefore assumed that the magnets had been stabilized and would operate in linear recoil for demagnetizing fields between 0 and –2800 Oe. This linearity is reflected in the modified demagnetization characteristic of Figure 29 that was used in the FEA. Firstly, the fundamental open circuit flux linkage due to the permanent magnet system alone is calculated from the FEA solution without excitation currents in Figure 30 to be Ψ_m per pole = 0.029 Wb.

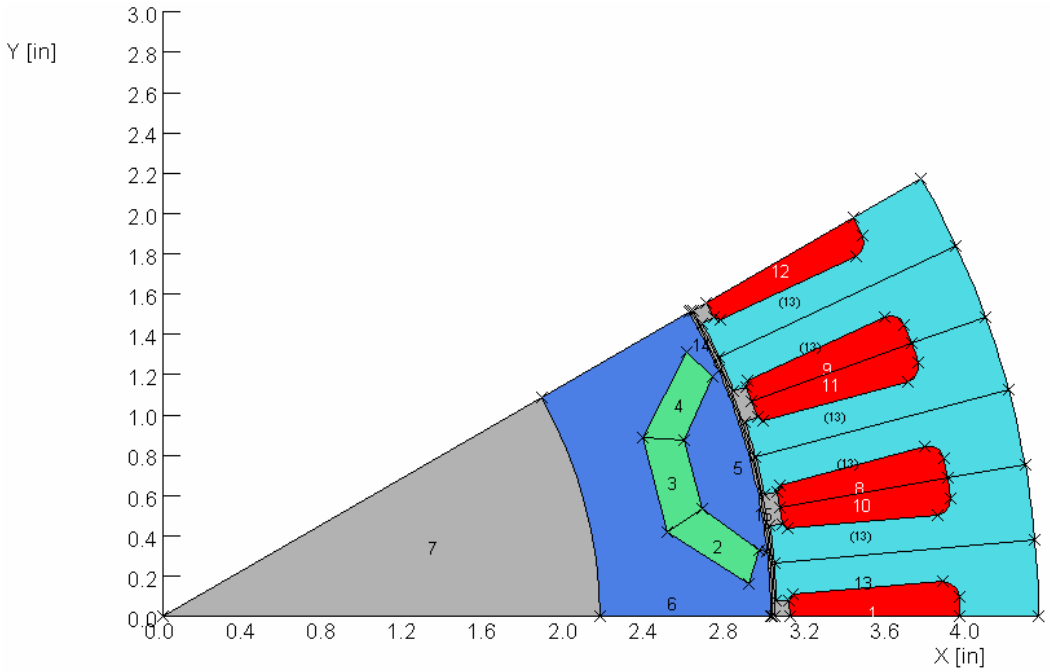

Fig. 27: Layout of anisotropic compression-molded NdFeB motor design in "Opera" FEA program

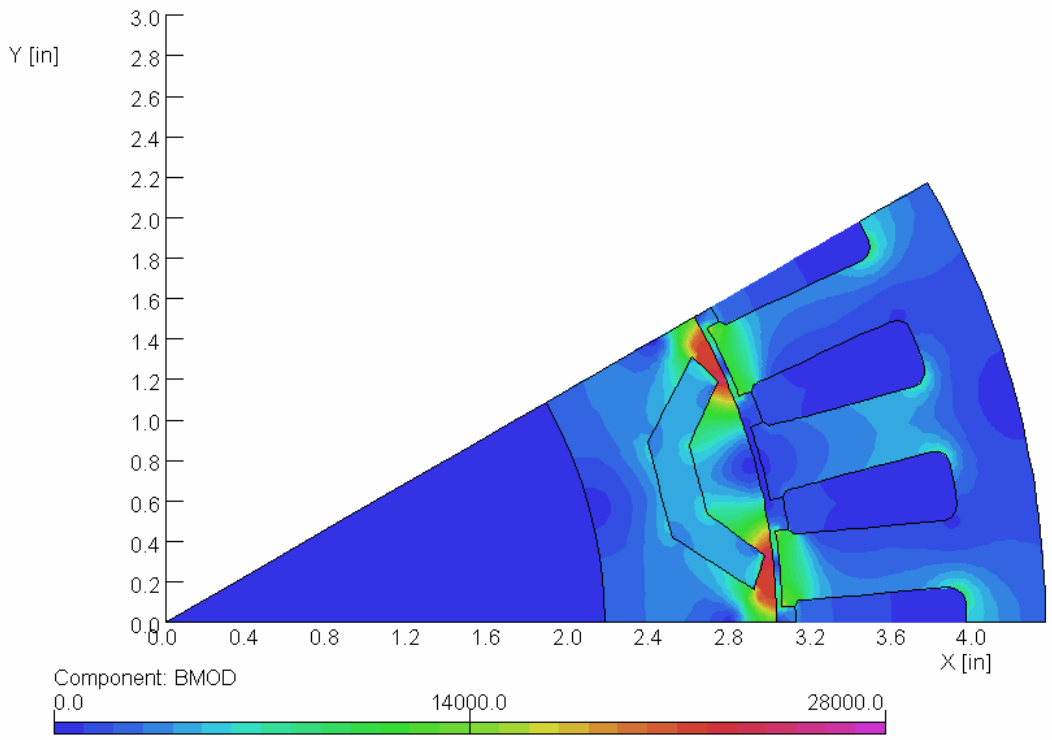

Fig. 28: Flux density in anisotropic compression-molded NdFeB motor design at peak demagnetization

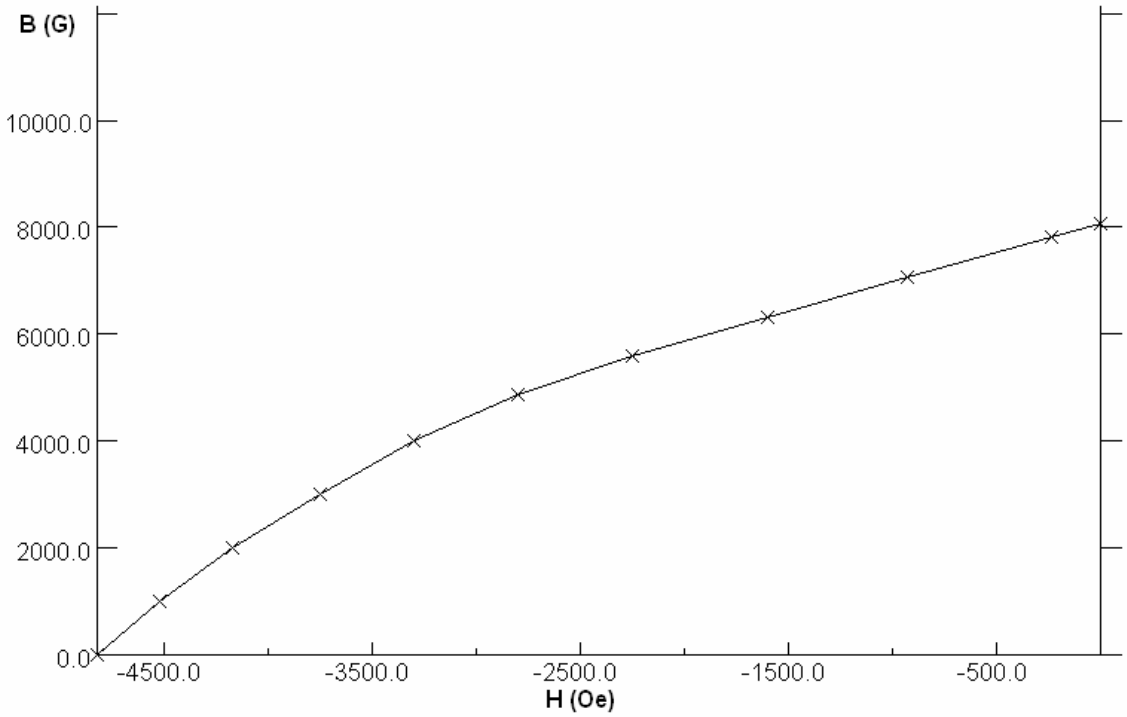

Fig. 29: Demagnetization characteristic of compression-molded Aichi MF25 magnet at 160°C after recoil to –2500 Oe

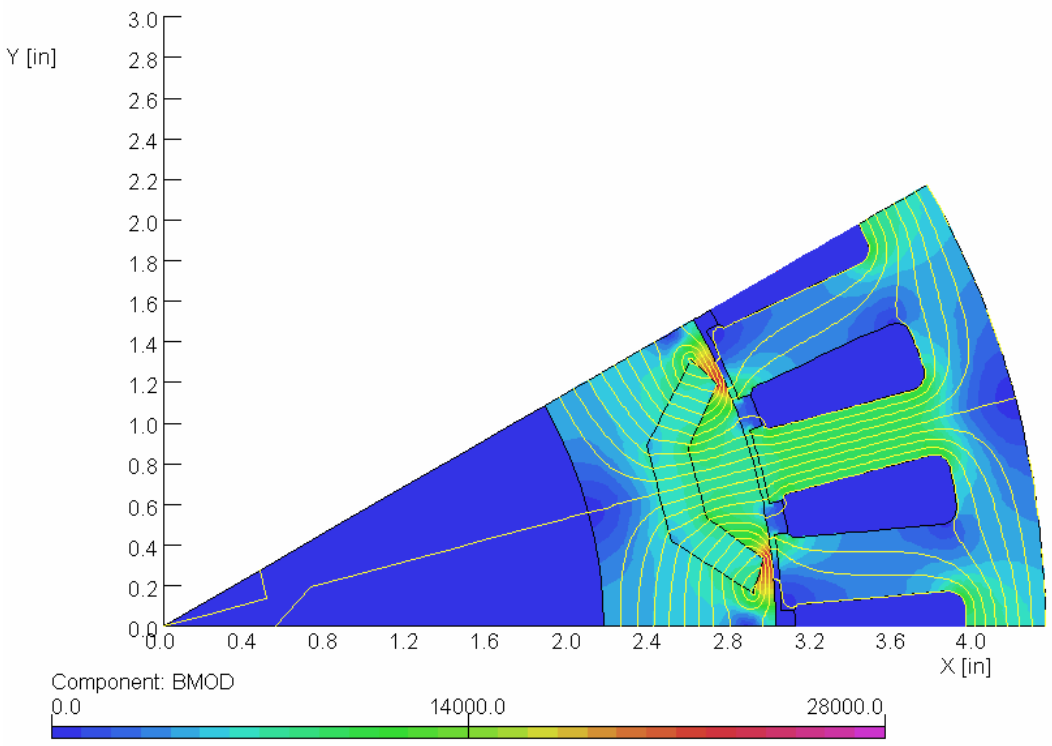

Fig. 30: Open circuit flux distribution in anisotropic compression-molded NdFeB motor design

The iterative FEA solution is again employed, adjusting I and γ and then re-computing the flux linkages until convergence is achieved. Despite the slightly thicker magnets compared to the sintered magnet types, the variations of inductances L_d and L_q versus I_d and I_q shown in Figure 31 are quite similar to those in the previous designs, even though the magnets centered on the d-axes are slightly thicker now.

The phasor quantities calculated for the motor using the compression-molded magnets are shown in Figure 32, the transitions in each curve (except for phase angle) again being relatively smooth. Capping of the voltage at 77.6V r.m.s., equivalent to the 200V d.c. minimum supply voltage, is achieved by advancing the phase angle γ from an initial 40^o towards 85^o at 10,000 rev/min. A noticeable improvement in the q-axis component $X_q I_q$ is again apparent in our new design compared to our calculations for the original UQM motor design in Figure 13, which collapsed at higher speeds but now holds up to provide reluctance torque up to full speed. And as shown in Figure 33, the motor is able to achieve its required peak operating profile over the full speed range without exceeding the allowable phase current of 400A.

The operating profile (Figure 2) also requires motor efficiency to exceed 93% at 20% of rated torque (i.e. 52 Nm) at speeds ranging from 1,000 to 10,000 rev/min.

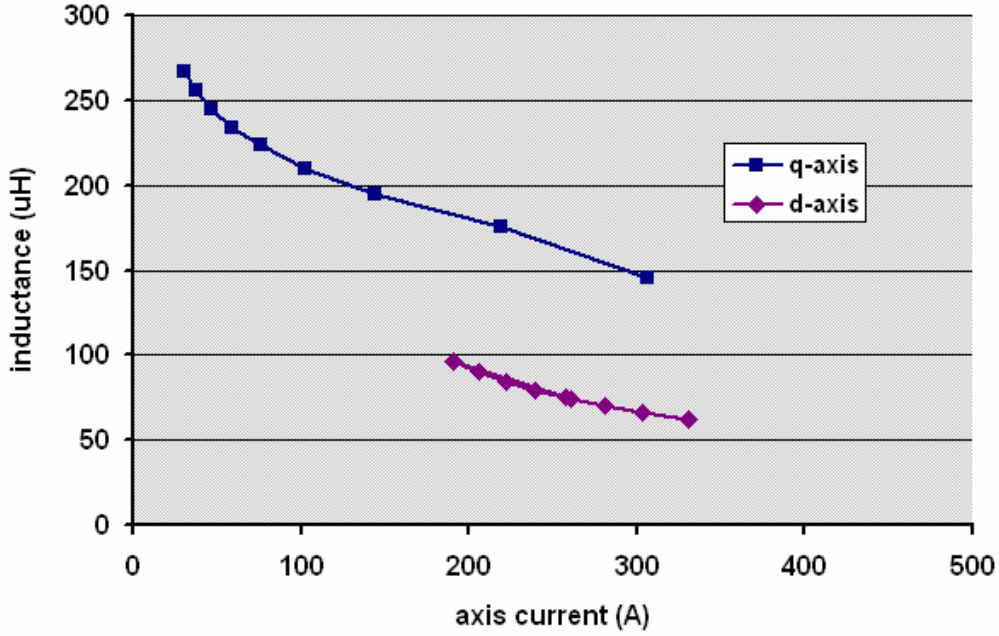

Fig. 31: Inductance vs. current in anisotropic compression-molded NdFeB motor design

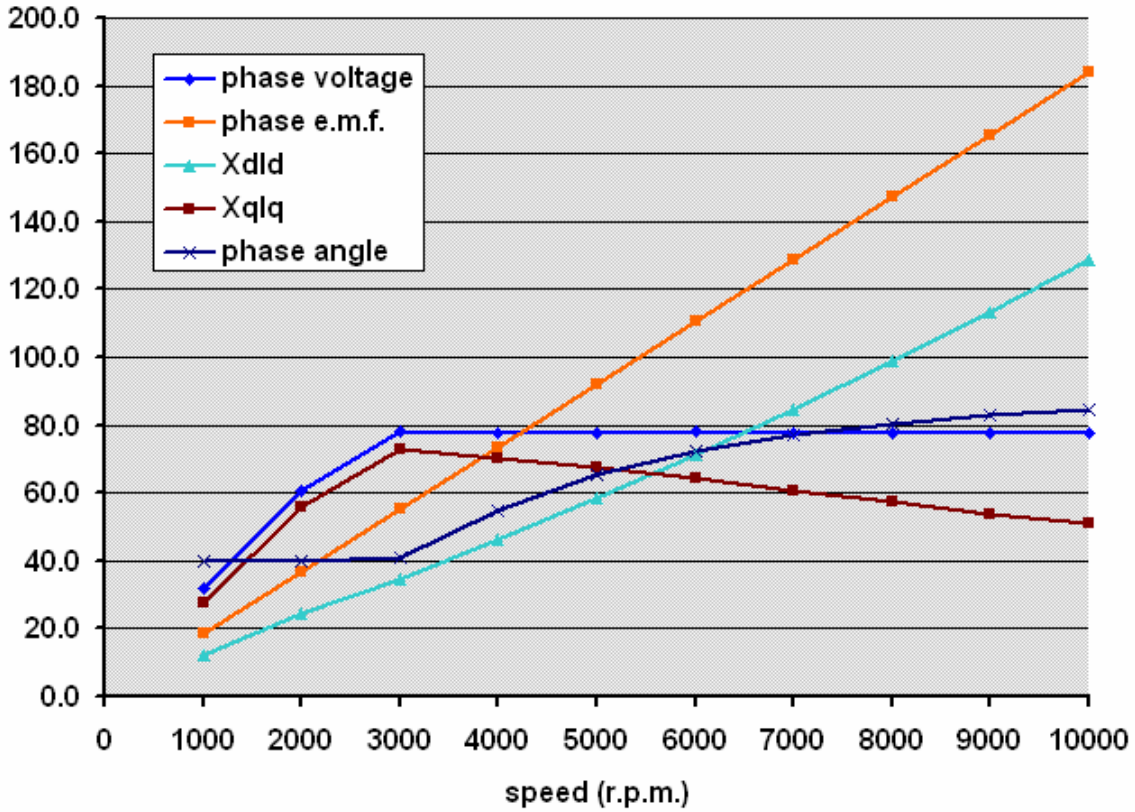

Fig. 32: Phasor quantities at 200V d.c. for anisotropic compression-molded NdFeB motor design

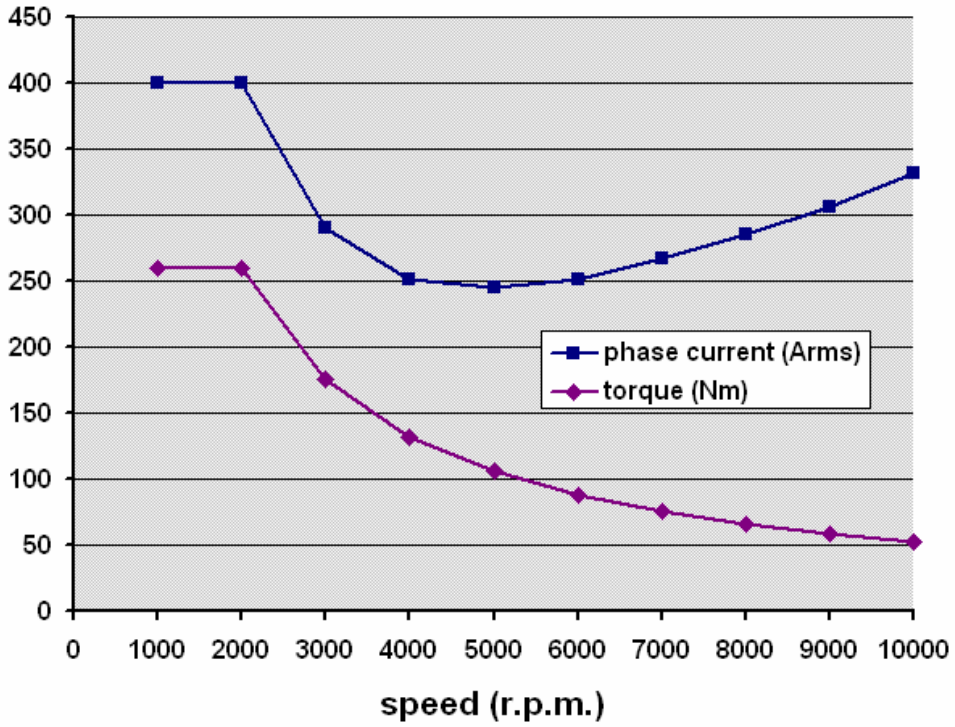

Fig. 33: Current profile at 200V d.c. for anisotropic compression-molded NdFeB motor design

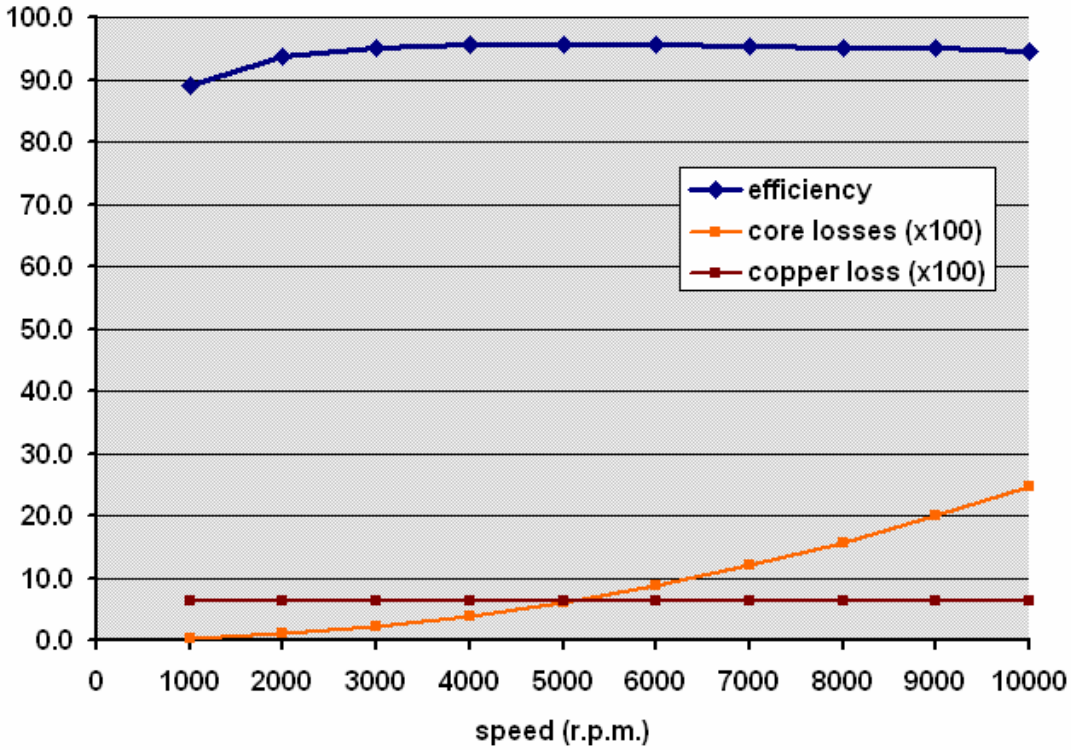

Fig. 34: Efficiency at 325V d.c. for anisotropic compression-molded NdFeB motor design (20% torque, 52 Nm)

This efficiency is calculated at the nominal 325V d.c. supply voltage, and allowing for a 10V d.c. voltage drop in the inverter, the corresponding r.m.s. voltage per phase is 128.6V. In this anisotropic compression-molded NdFeB motor design, 52 Nm is achieved over the entire 1,000 to 10,000 rev/min range with a constant phase angle γ of 60.8^o and a constant phase current of 145A — 5A less than in the modified UQM motor design using sintered NdFeB magnets. The I^2R power loss in the winding is constant over this speed range, but the core losses in the magnetic circuit vary as a function of both the peak field distribution (B) and the speed as discussed in Section 2.1. Figure 34 shows that the target efficiency of >93% is achieved from 2,000 to 10,000 rev/min, falling below this to 89% at 1,000 rev/min. A maximum efficiency of 95.6% is reached at about 5,000 rev/min and 52 Nm.

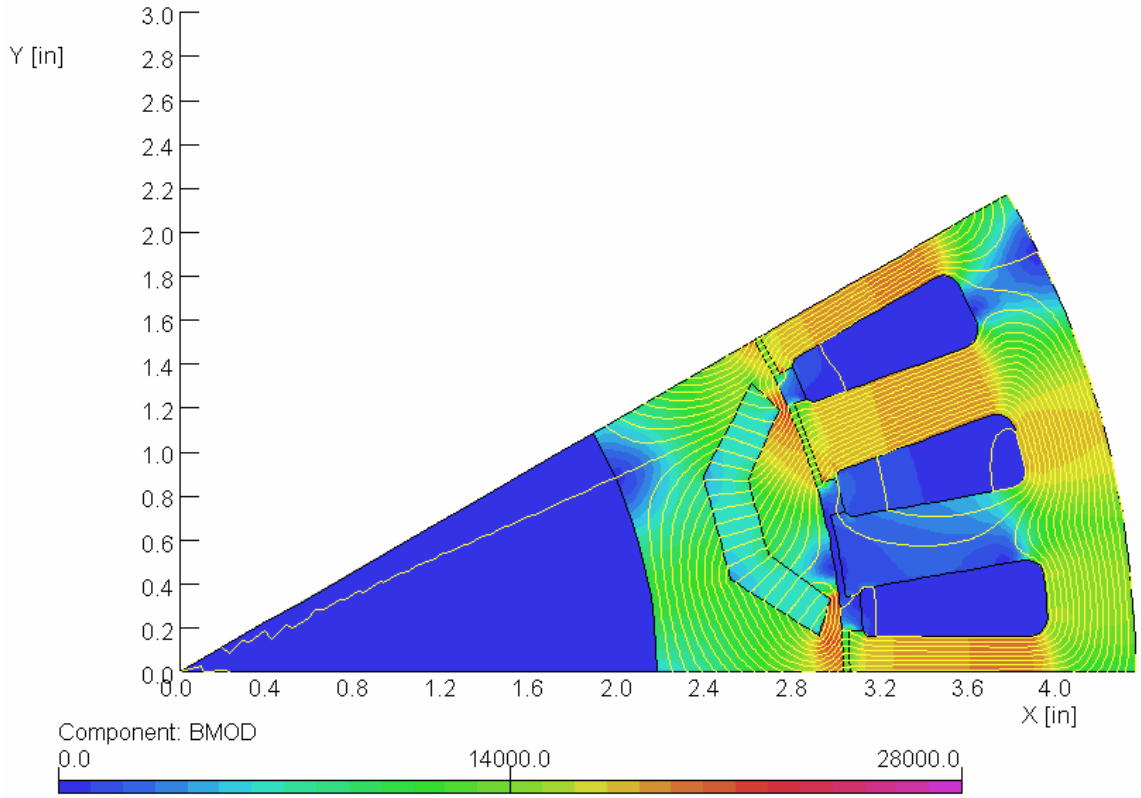

Fig. 35: Maximum electromagnetic stress in anisotropic compression-molded NdFeB motor design

The foregoing flux density plots again show that the greatest concentration of magnetic flux is at the narrow regions in the rotor that bridge the magnet slots with the rotor circumference, whose minimum thickness has been specified as 0.040". To check that the mechanical stress developed in these regions should not affect the integrity of the rotor, FEA is used to calculate the component of this stress which is due to electromagnetic forces developed in the magnetic circuit. With the maximum allowable phase current applied to the winding, the phase

angle γ is varied until the maximum electromagnetic component of stress is found in the position shown in Figure 35. The corresponding flux density distribution along this 30° pole pitch section of the rotor surface is shown in Figure 36. Across the 0.040" bridge section, this yields the component of stress due to electromagnetic forces of 7.70 MPa. The geometry of the rotor section above the magnet slots is unchanged, so the other component of stress due to centrifugal force at 10,000 rev/min is again 112.60 MPa, giving a total stress across the 0.040" bridge section of 120.3 MPa. This is safely within the 350 MPa yield strength of M19 electrical lamination steel.

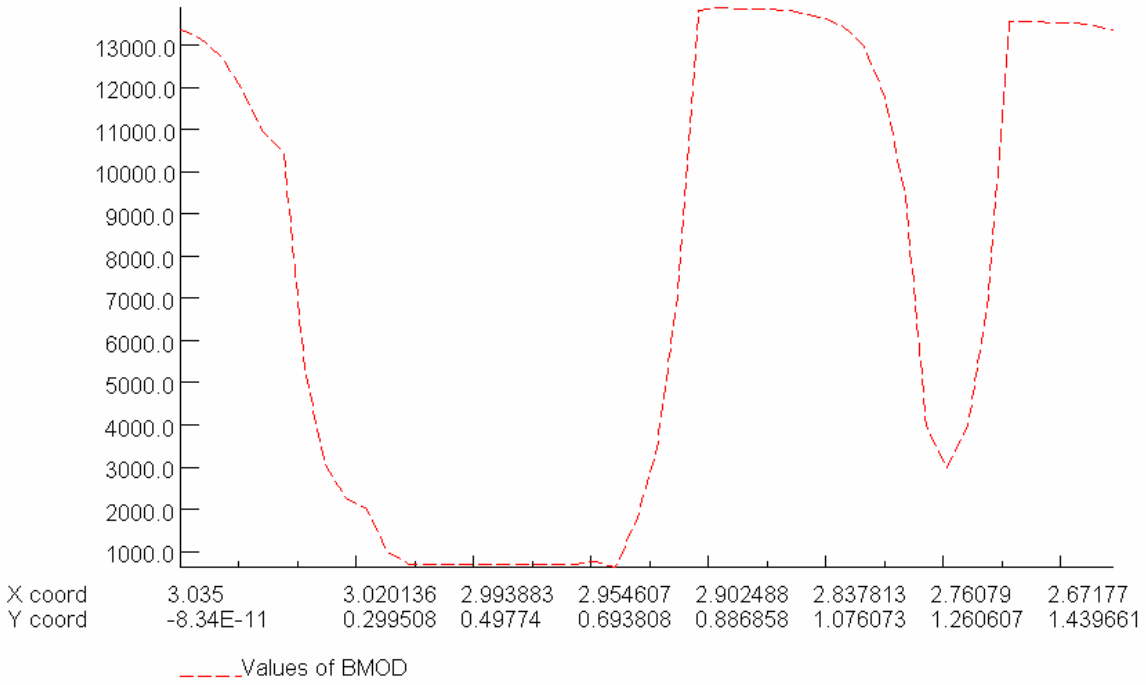

Fig. 36: Flux density distribution from one pole pitch for maximum electro-magnetic stress in anisotropic compression-molded NdFeB motor design

3.5: ISOTROPIC BONDED NdFeB

Isotropic bonded NdFeB magnets are well-known and have found broad commercial application, mainly in consumer electronics applications which require more modest magnetic performance at more modest operating temperatures. The most common process to make stable powder for subsequent compounding and molding is rapid solidification, specifically by melt spinning. Magnequench has had the most notable success in commercializing state-of-the-art NdFeB powder to manufacturers of isotropic compression- and injection-molded magnets, thanks to early protection by their 1983 invention of both the NdFeB composition and its melt-spinning process. However, only a few grades of melt-spun NdFeB powder have been developed to perform above 150°C, the most suitable being MQP-14-12.

The isotropic nature of this powder yields a much reduced energy density compared to anisotropic sintered NdFeB; for example, a compression-molded MQP-14-12 magnet has a room temperature $(BH)_{max}$ of only 9 MGOe, compared to 29 MGOe for the N30UH grade sintered magnet or 24 MGOe for the compression-molded MF25 magnet discussed earlier. For isotropic NdFeB to be considered at all for this IPM application, it would have to be on merits other than its magnetic performance. The most compelling reason is the ability to form this material directly into the IPM rotor slots without the need for magnetic orientation, as would be possible by injection-molding. But this further reduces magnet's energy density, as does the need to use a high temperature binder such as PPS instead of nylon. The powder remanence of 8,200 Gauss translates to a B_r of 5,000 Gauss when diluted at 61vol% for an injection-molded magnet (Figure 37).

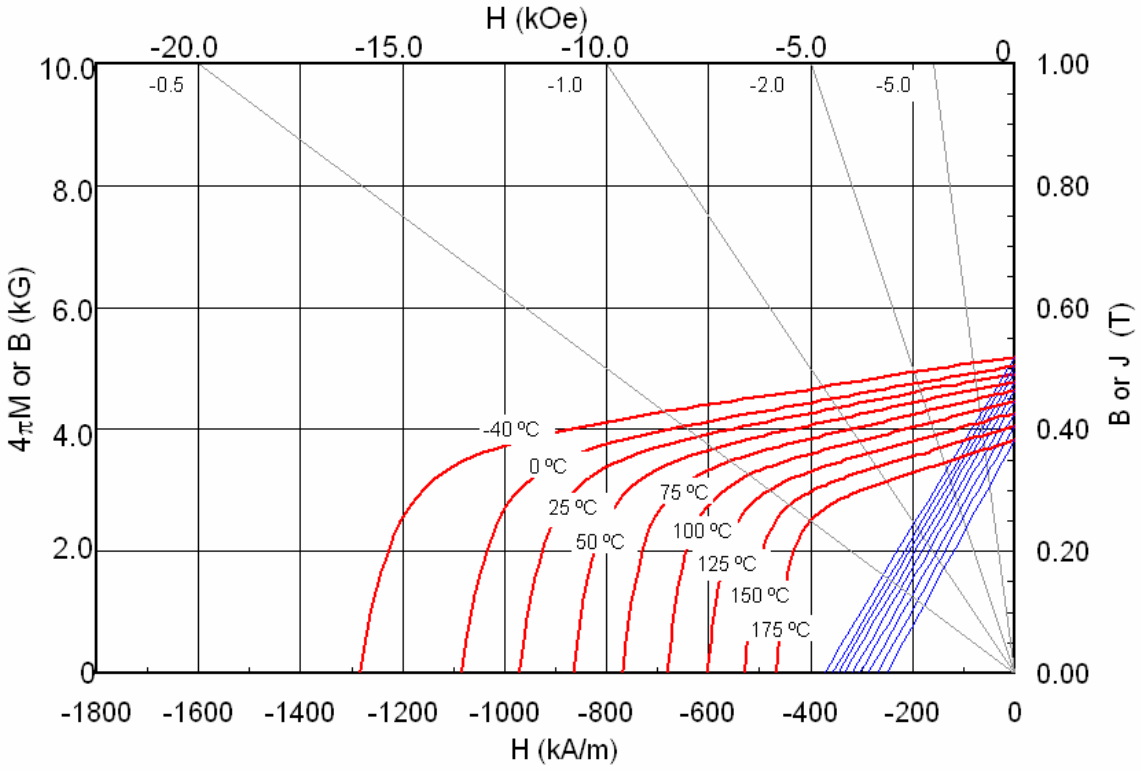

Fig. 37: Demagnetization characteristics of MQP-14-12 grade NdFeB, injection-molded with PPS at 61vol%

3.6: IPM MOTOR DESIGN WITH ISOTROPIC BONDED NdFeB

Several variations on the motor design were tried using injection-molded MQP-14-12 magnet material with a demagnetization characteristic derived at 160°C to have a B_r of 4,050 Gauss (Figure 38). To provide these magnets with adequate protection against demagnetization and to preserve the machine's reluctance

motor performance, it was necessary to substantially increase the effective magnet thickness by using two U-shaped sections as shown in Figure 39.

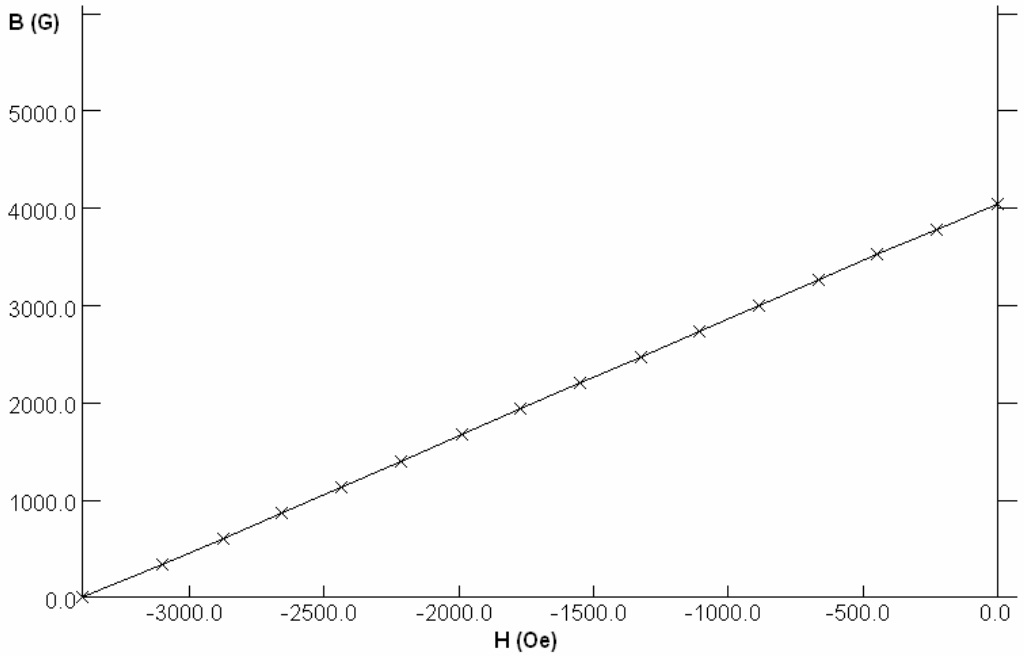

Fig. 38: Demagnetization characteristic of injection-molded MQP-14-12 magnet at 160°C

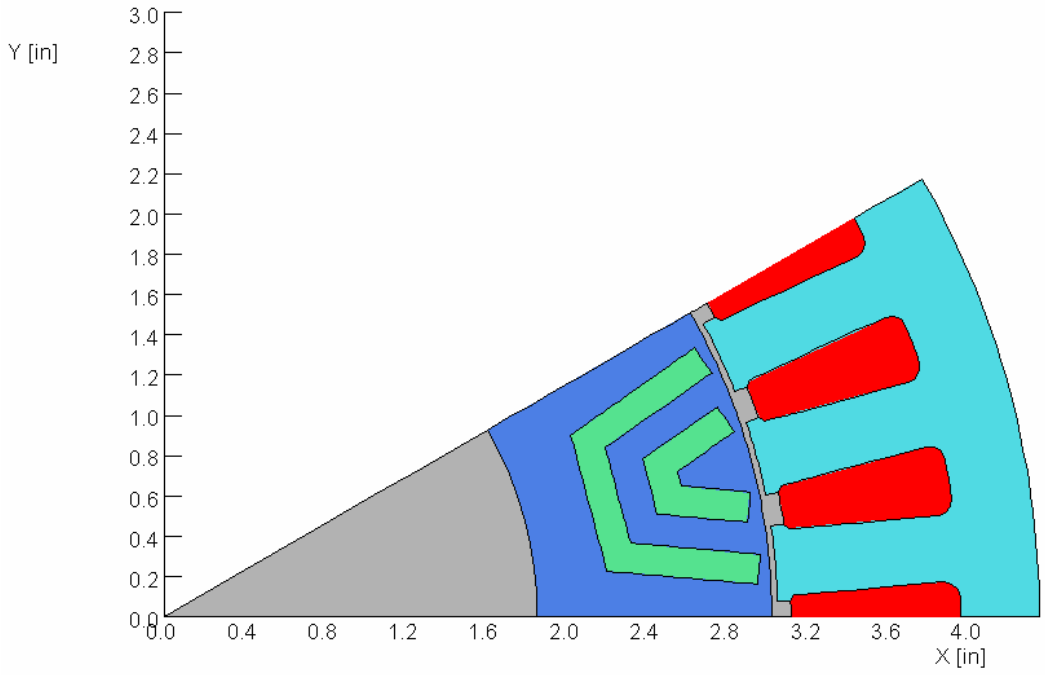

Fig. 39: Layout of isotropic injection-molded NdFeB motor design in "Opera" FEA program

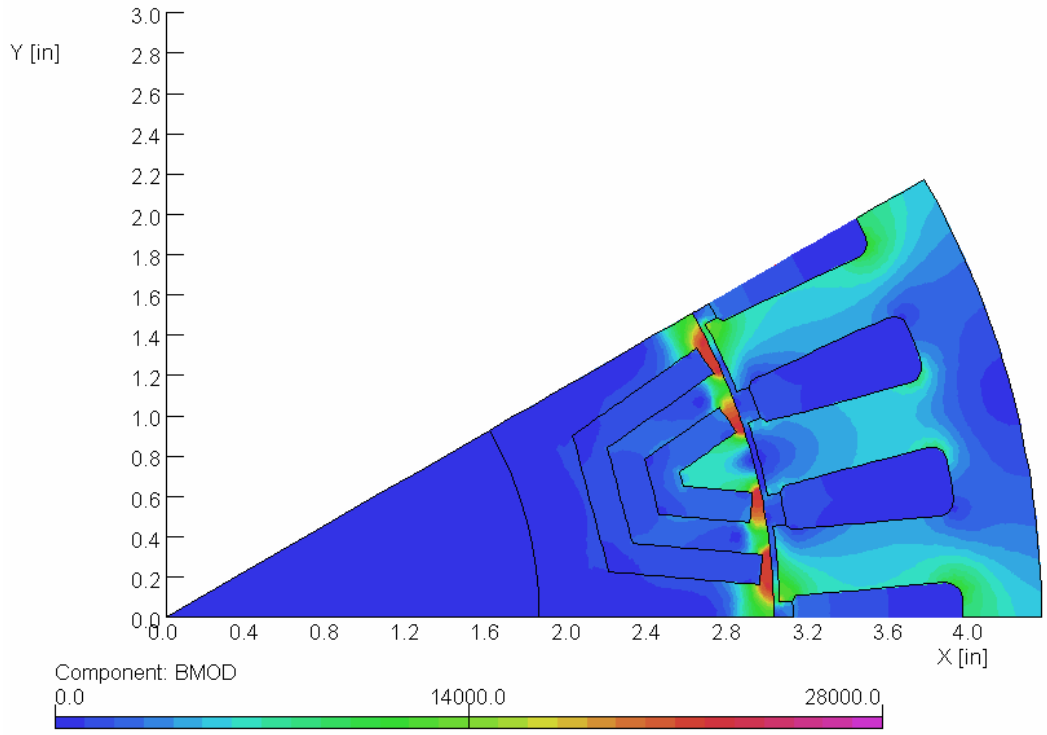

Fig. 40: Flux density in isotropic injection-molded NdFeB motor design at peak demagnetization

With the maximum allowable excitation of 1200 Ampère-turns in a coil applied directly towards the magnets along the d-axes (when γ approaches 90°), the corresponding FEA in Figure 40 shows the flux density magnitude distribution using the 160°C magnet characteristic. These magnets have a constant thickness of 0.150" in each section (0.030" total), which had been adjusted until a maximum demagnetizing field of about –2400 Oe was obtained, not enough to drive the magnet from its linear region in Figure 38 and into recoil.

But the relative weakness of this isotropic bonded magnet system significantly reduces the fundamental open circuit flux linkage, calculated from the FEA solution without excitation currents (Figure 41) to be Ψ_m per pole = 0.0194 Wb. Unfortunately, Ψ_m directly affects and consequently reduces the permanent magnet alignment component of the motor's torque. The iterative FEA solution is again employed, adjusting I and γ and then re-computing the flux linkages until convergence is achieved. The variation of inductance L_q versus I_q shown in Figure 42 is quite similar to those in the previous designs, but because the thickness of the magnets centered on the d-axes has changed significantly, so too has the variation of L_d versus I_d, drastically reducing their difference ($L_q - L_d$) which governs the reluctance component of the motor's torque. So both components of this IPM motor's output torque are inherently reduced as a result of designing with a much weaker permanent magnet material. While the goal is for this design to achieve its required peak operating profile over the full speed range both within an allowable phase current and within the prescribed weight

and volume, it was found it could only stay within these limits by developing about 55% of the required output torque.

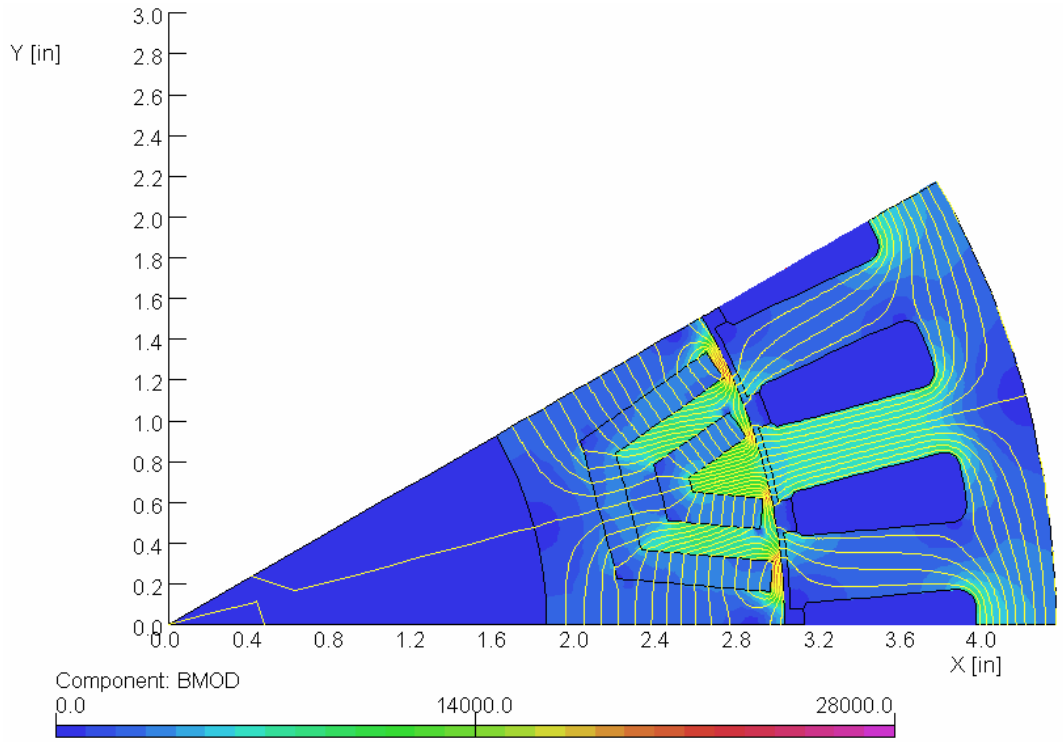

Fig. 41: Open circuit flux distribution in isotropic injection-molded NdFeB motor design

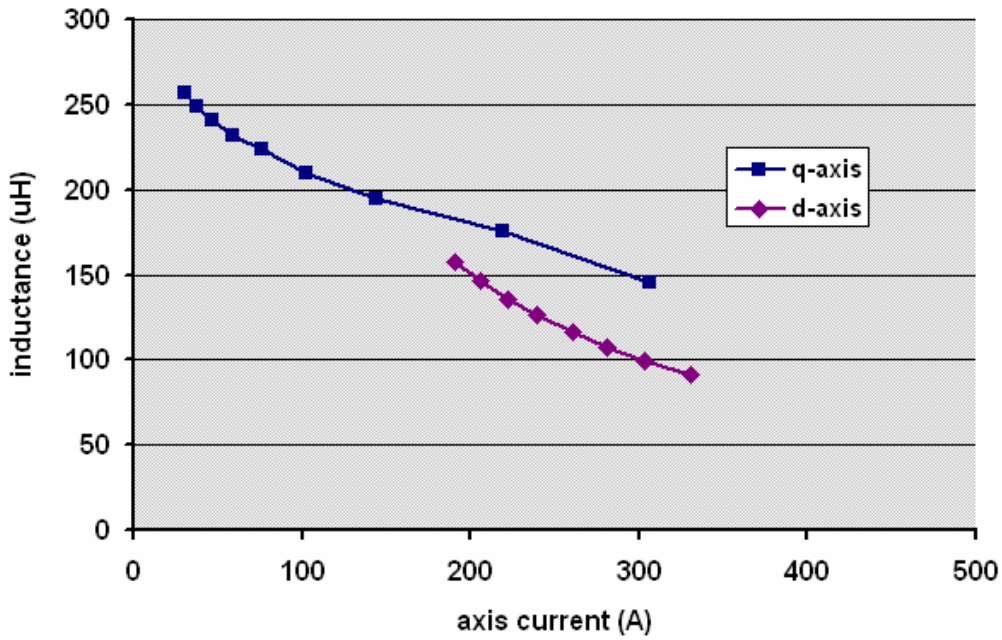

Fig. 42: Inductance vs. current in isotropic injection-molded NdFeB motor design

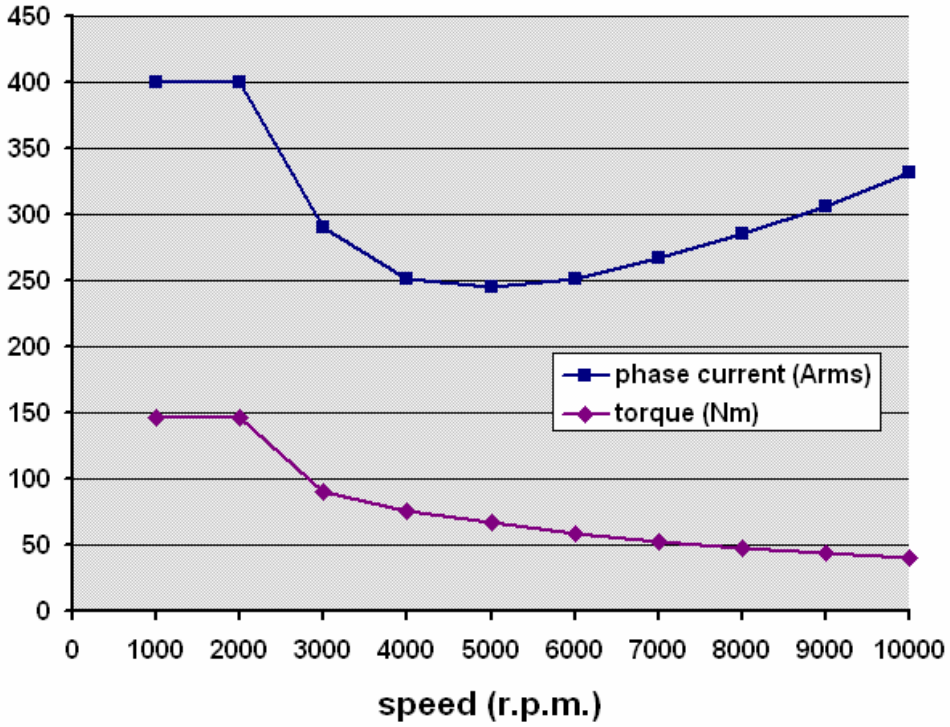

Fig. 43: Torque and current profiles at 200V d.c. for isotropic injection-molded NdFeB motor design

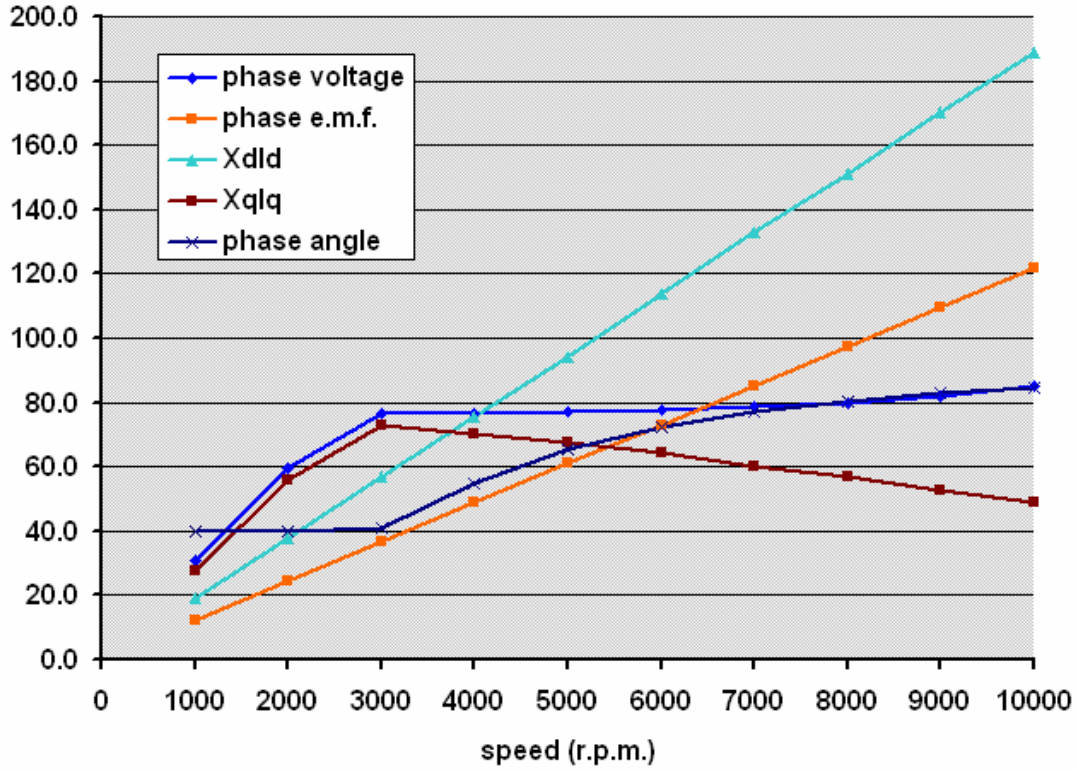

Fig. 44: Phasor quantities at 200V d.c. for isotropic injection-molded NdFeB motor design

The consequent reduced peak operating torque profile shown in Figure 43 is achieved over the full speed range without exceeding the allowable phase current of 400A. The corresponding phasor quantities calculated for the motor using the injection-molded magnets are shown in Figure 44, the transitions in each curve (except for phase angle) again being relatively smooth. The phase angle γ was allowed to advance from an initial 40^o towards 85^o at 10,000 rev/min, as it did with the previous successful design using anisotropic compression-molded magnets, but in this case it was not possible to cap the voltage at 77.6V r.m.s (equivalent to the 200V d.c. minimum supply voltage) over the full speed range – this had to be allowed to rise steadily from 5000 rev/min to 85 V r.m.s. at 10,000 rev/min.

For the motor to develop the required peak operating profile that was shown in Figure 1, our design calculations indicate that the stack length would have to increase from 3.4" used in all the foregoing designs to 6.1", an 80% gain in active volume if the same lamination profiles are used. Therefore, this IPM motor design is not viable in that it falls far short of its requirements for power-to-weight and power-to-volume ratios. Because of this, no further design variations were performed using isotropic injection-molded NdFeB magnets, which would have had to include further iterations on the winding layout to account for the now greater phase resistance. It is worth noting that this result concurs with our previous experience designing IPM electric vehicle drive motors, which have also needed much greater stack lengths when using injection-molded NdFeB, the rotors even needing to be assembled from multiple sections.

4: COST STRUCTURES AND TRADEOFFS

4.1: VOLUME AND WEIGHT COMPARISON

The motor specifications given in Table 1 stated the required peak power-to-weight and peak power-to-volume ratios for active materials to be >2.75 kW/kg and >12.5 kW/liter respectively. These "active materials" consist of the stator core, rotor core, stator winding and magnets, and thus correspond with the components which constitute the motor's "electromagnetic" design of the present study. Peak power of 55 kW means that the maximum weight of these active materials must be 20 kg and their maximum volume must be 4.4 liters.

Our two viable alternatives to the original UQM motor design used N30UH grade sintered NdFeB magnets and MF25 grade compression-molded NdFeB magnets, the layouts for which were shown in Figures 16 and 27 respectively. These new designs both meet the peak performance requirements and are unchanged from the original UQM layout in respect of their overall dimensions. Therefore, these designs both achieve the same original peak power-to-volume ratio for active materials. In the *most* conservative calculation described by UQM, and using the more realistic allowance of 0.22 in. for each end-turn length, the volume occupied by active materials is 3.7 liters and the power-to-volume ratio is 14.7 kW/liter, comfortably meeting the 4.4 liters and 12.5 kW/liter threshold requirements. In contrast, a design using MQP-14-12 injection-molded NdFeB magnets having the profile shown in Figure 39 would require a smaller bore radius by 0.32 in., and an increase in stack length by 2.7 in. – the active material volume would then be 5.2 liters yielding a peak power-to-volume ratio of 10.55 kW/liter, neither of which meet the performance goals.

Table 5: Weights of active material components

Part description	Weight of parts/unit (kg)		
	Original UQM design*	New design, sintered NdFeB	New design, compression-molded NdFeB
Stator lamination stack:	9.82	9.19	9.19
Rotor lamination stack:	4.55	5.40	4.62
Magnets:	1.01	0.65	1.39
Stator winding (copper):	3.18	3.89	3.89
Total weight of active materials:	18.55	19.12	19.09
Peak power-to-weight ratio for active materials:	2.97 kW/kg	2.88 kW/kg	2.88 kW/kg

* from Table 14 of the UQM Final Report

The final motor design by UQM met the required peak power-to-weight ratio for active materials with 2.97 kW/kg, according to component weights that they reported. So too do our two viable alternatives with N30UH grade sintered NdFeB magnets and MF25 grade compression-molded NdFeB magnets with 2.88 kW/kg for either, as detailed in Table 5 from our calculations of individual component weights. Notice the benefit in reduced weight of the sintered NdFeB magnets which accrues from our adjustments to the original UQM design, and also the magnet weight penalty incurred to compensate for dilution of the magnetic material in compression-molded NdFeB. But in all cases, the ratios of these component weights approximately agree with the projections given in Table 10 of the 2010 FreedomCAR specification[6].

4.2: PROCESS AND MANUFACTURING COMPARISON

NdFeB magnets are not, in fact, ternary alloys of just these three elements, but comprise a variety of partial substitutions and additives that provide a range of materials (grades) with widely differing properties. We already saw in Section 3.1 that there can be a tradeoff between the remanence B_r and intrinsic coercivity H_{ci} of a magnet, and that its stable operating temperature can also be raised in conjunction with H_{ci}. As illustrated in Figure 45, all the elements for a sintered NdFeB material are combined as an ingot, which is then crushed, milled to a powder, and then aligned in an applied magnetic field. This alignment occurs in

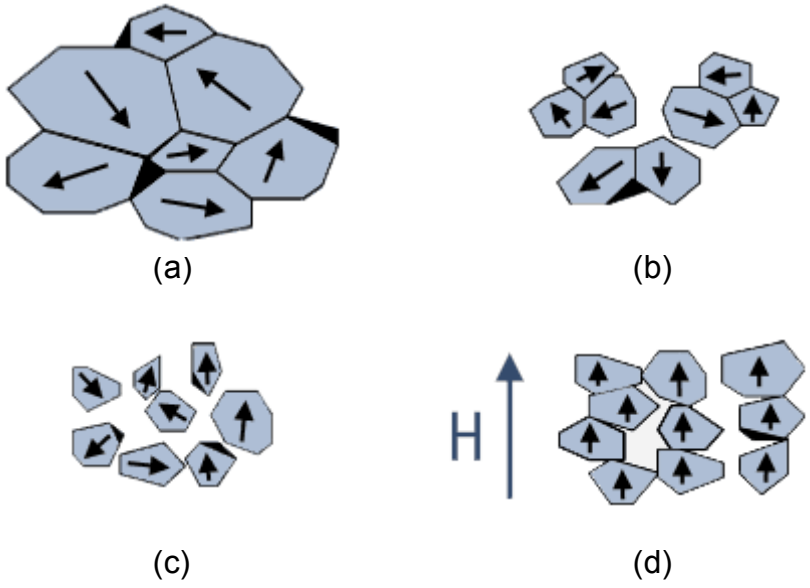

Fig. 45: Sintered NdFeB is prepared by crushing the alloy (a)→(b), milling to powder (b)→(c), and aligning in an applied magnetic field (c)→(d)

[6] *Electrical and Electronics Technical Team Roadmap*, FreedomCAR Fuel Partnership, November 2006.

either an isostatic press or a die press, the most basic method being the latter embodied using an axial aligning field as shown in Figure 46. A simple toroidal coil spans the die cavity to provide a relatively uniform field within it, without impinging upon the press action of the upper and lower punches. This method lends itself to the use of simple die cavities that can directly produce rectangular blocks to the near net shape required for this IPM application. It was the first method to be employed when sintered NdFeB production was established in China, and is still the most commonly and reliably used there. The NdFeB grades produced by San Huan which were summarized in Table 4, including the N30UH grade that has been selected, are all produced using axial aligning presses.

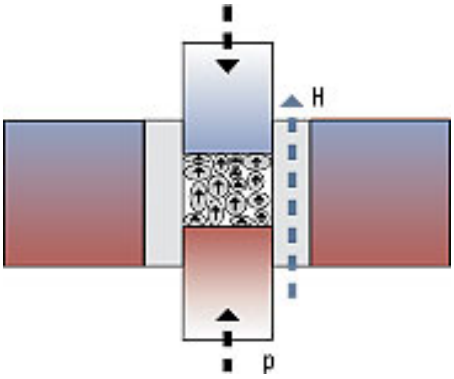

Fig. 46: Axial aligning press

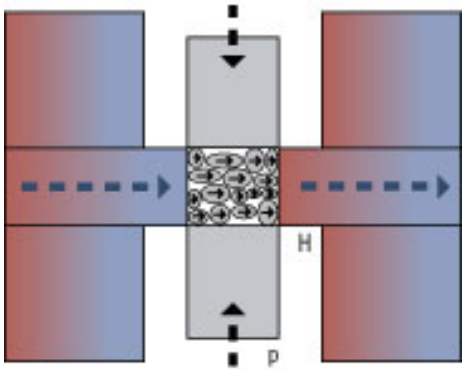

Fig. 47: Transverse aligning press

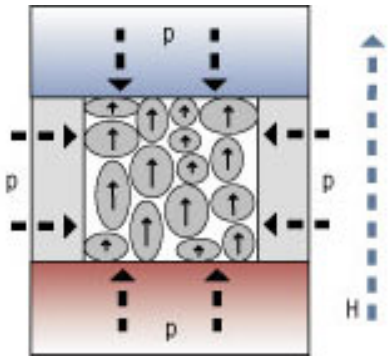

Fig. 48: Isostatic press with pre-aligned powder

Better magnetic alignment and/or densification could be achieved using either of the following methods, which provide about 6% greater remanence for any given alloy composition compared to axial-pressed magnets. The die press using a transverse aligning field from a pair of external toroidal coils as shown in Figure 47 allows better saturation of the die cavity, whereas the isostatic press illustrated in Figure 48 achieves better densification of powder within a flexible cavity which has been pre-aligned with a field. Neither of these two methods can directly produce the relatively thin rectangular block to the near net shape required for this IPM application, but instead would require that much larger blocks be made and subsequently sliced into multiple thinner parts. But our studies have shown that, because the IPM motor does not function solely as a traditional permanent magnet motor, its design would not really benefit from this slight gain in remanence. Although this may change in years to come as China's rare earth magnet industry matures further, the most economical sintered NdFeB parts that would be supplied today are made to near net shape using axial alignment. The fully-dense magnets are then sintered at a temperature in the

range 1100–1300°C, machined to their final dimensions and lastly magnetized. With three magnets comprising each pole (regions 2 through 4 in Figure 16), the near net shape for each individual magnet is shown in Figure 49. In this modified UQM motor design, the long 0.10" edges of these magnets will be slightly beveled by 19.5° during final machining.

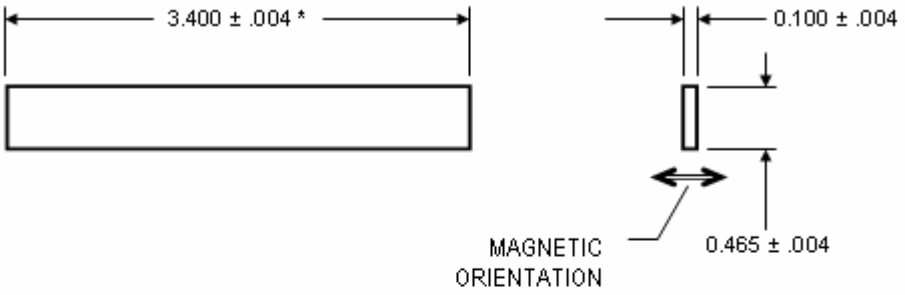

RECTANGULAR MAGNET BLOCK:

QUANTITY: 7.2 million/year

Magnet type:	Sintered Neo (N-30UH)
B_r minimum:	10.8 kG
H_{ci} minimum:	25.0 kOe
$(BH)_{max}$:	30 MGOe
Coating:	none
* If necessary, length may be divided into N pieces and quantity increased N times	
Dimensions in inches	

Fig. 49: Drawing of N30UH grade sintered NdFeB magnet (near net shape) for the modified UQM motor design

Because these high energy magnets are brittle, it is preferable to assemble and bond them into the rotor slots of the IPM motor in their unmagnetized state, and to subsequently magnetize the fully assembled rotor. This is possible because the magnetization behavior of sintered NdFeB is based on a mechanism called "nucleation", in which the grain boundaries are composed of deviations from the primary $Nd_2Fe_{14}B$ composition that allow relatively easy movement of the domain walls during magnetization, while subsequently resisting domain reversal to provide high H_{ci}. As illustrated in Figure 50 for a grade N30SH sintered NdFeB magnet, a relatively modest field strength of >20 kOe is sufficient to magnetize the material to saturation and establish the proper major demagnetization characteristic. The N30UH grade used in our IPM motor would behave in a quite similar fashion, only needing a magnetization field strength of >25kOe. A magnetization fixture providing this field level can certainly be designed to saturate the magnets even though they are buried in slots within the steel rotor

structure, with proper magnetic orientation within each magnet already provided by the prior alignment imparted during the pressing operation.

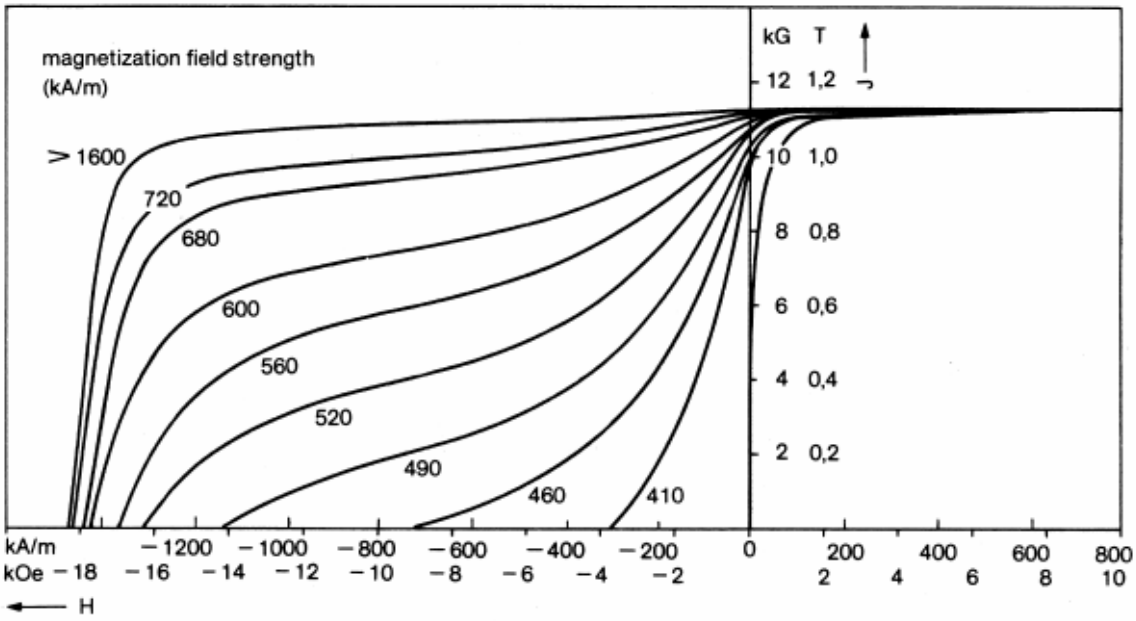

Fig. 50: Magnetization characteristics for N30SH grade NdFeB

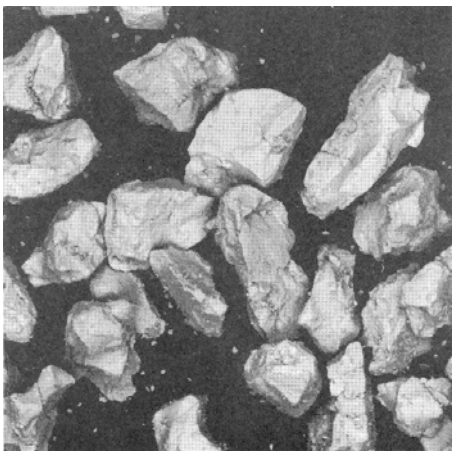

Fig. 51: HDDR powder made by Aichi Steel

As an alternative to sintered NdFeB we have proposed using anisotropic bonded NdFeB introduced in Section 3.3, specifically the "MAGFINE" grade MF25 powder (Figure 51) which is made by Aichi Steel Corporation using modifications to the hydrogenation, disproportionation, desorption and recombination ("HDDR") process. In fact, the first stage of this process is quite similar to the hydrogenation which is commonly used to aid reduction of alloy in the sintered NdFeB process (stages a through c in Figure 45), but expands upon the basic HDDR process which was invented by Mitsubishi Materials Corporation[7]. A basic attribute claimed for the new Aichi process is its added complexity compared to Mitsubishi's original one, amounting to three separate stages of processing for the powder as illustrated in Figure 52. Aichi's first hydrogenation step at low temperature (#2 in Figure 52b) produces the hydride that stores hydrogen needed in advance of phase transformation, the second hydrogenation step adds heating to elevated temperature and produces a mixture of NdH_2, Fe and Fe_2B from the hydride (#3

[7] T. Takeshita, R. Nakayama and T. Ogawa, "Rare earth-iron-boron magnet powder and process for producing same", *U.S. Patent 5,110,374*, May 5, 1992.

in Figure 52b), and the desorption step then produces a fine grained microstructure of $Nd_2Fe_{14}BH_x$ with a high degree of crystallographic orientation (#4 in Figure 52b). Aichi's process then adds a further heat treatment step (#6 in Figure 52b) in which additional elements, specifically dysprosium (Dy), are diffused into the powder, which then recombines into $(Nd,Dy)_2Fe_{14}B$.

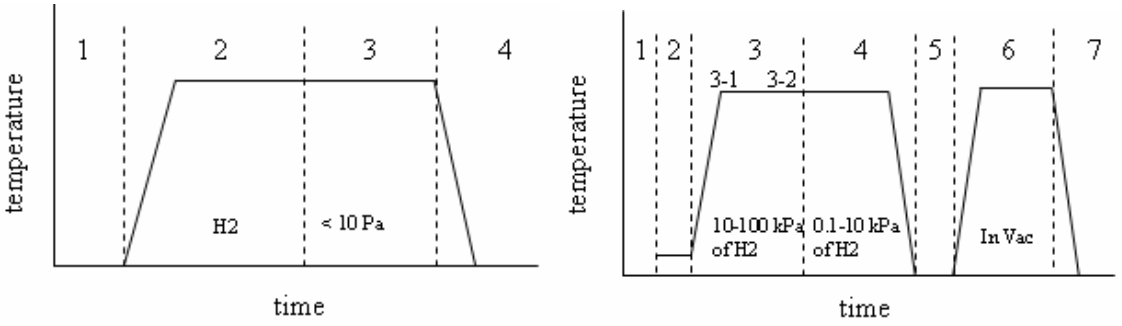

Fig. 52: HDDR process for making anisotropic NdFeB powder of (a) Mitsubishi Materials Corporation and (b) Aichi Steel Corporation

While Aichi's process is admittedly relatively complex, the powder produced is then amenable to quite common compounding and molding techniques. To make it suitable for compression-molding, the MF25 powder is passivated by blending it into compound with epoxy resin (Figure 51), effectively coating the powder with the liquid epoxy at a typical volume fraction of 78.5%. The compound is thermosetting after being molded in an orienting die press, which could be configured either as an axial aligning press of Figure 46 or as a transverse aligning press of Figure 47, the choice depending upon the shape and orientation of the specific part to be molded.

The layout for our IPM motor design in Figure 27 shows three compression-molded magnets comprising each pole (regions 2 through 4), the side sections tapering slightly towards the outer ends in order to stabilize them uniformly against demagnetizing fields. To simplify the shape for the purpose of obtaining a realistic manufacturer's quotation, the composite magnet was approximated to a radially-oriented 120^o arc segment having an averaged radial thickness, as shown in Figure 53. This shape and magnetic orientation will need to be made in a transverse aligning press, with compression along the 3.4" length dimension of the part. These bonded magnet segments are assembled and bonded into the rotor slots of the IPM motor in the same manner as with the sintered magnets. The fully assembled rotor can be magnetized as a whole, again using a relatively modest field strength of >15 kOe to saturate the magnets and establish their proper major demagnetization characteristic.

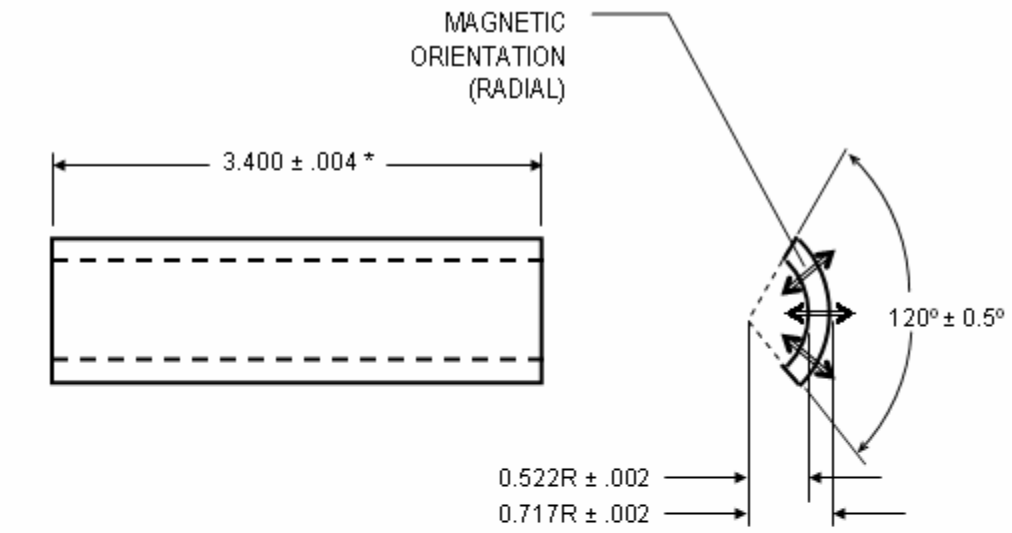

RADIALLY-ORIENTED ARC MAGNET:

QUANTITY: 2.4 million/year

Magnet type:	Compression-bonded anisotropic Neo (Aichi MF25)
B_r nominal:	11.0 kG
H_{ci} nominal:	14.0 kOe
$(BH)_{max}$:	25 MGOe
Coating:	none
* If necessary, length may be divided into N pieces and quantity increased N times	
Dimensions in inches	

Fig. 53: Drawing of MF25 grade magnet for anisotropic compression-molded NdFeB motor design

Given the foregoing discussion, it is apparent that the difference between the costs of manufacturing anisotropic sintered versus compression-molded NdFeB magnets for the IPM motor will lie both in the powder preparation and in its consolidation into magnet. This, together with the raw materials costs, should be reflected in any difference in the manufacturers' quotations.

4.3: COST COMPARISON AND TRENDS

The magnets we are using are based upon the $Nd_2Fe_{14}B$ ternary alloy composition, with various partial substitutions and additives to provide the specific properties that are required for this application. Approximate actual compositions for the specific grades we have selected are given in Table 6, ignoring very minor elements comprising <1wt%. Obviously neodymium is the

major contributor to raw materials costs, but dysprosium and cobalt also cannot be ignored.

Table 6: Compositions of certain NdFeB alloys

Anisotropic magnet type	Grade	Composition (wt%)				
		Nd	Dy	Co	Fe	B
Sintered:	N30UH	31.0	4.5	2.0	61.5	1.0
Compression-molded:	MF25	23.8	1.6		73.7	0.9

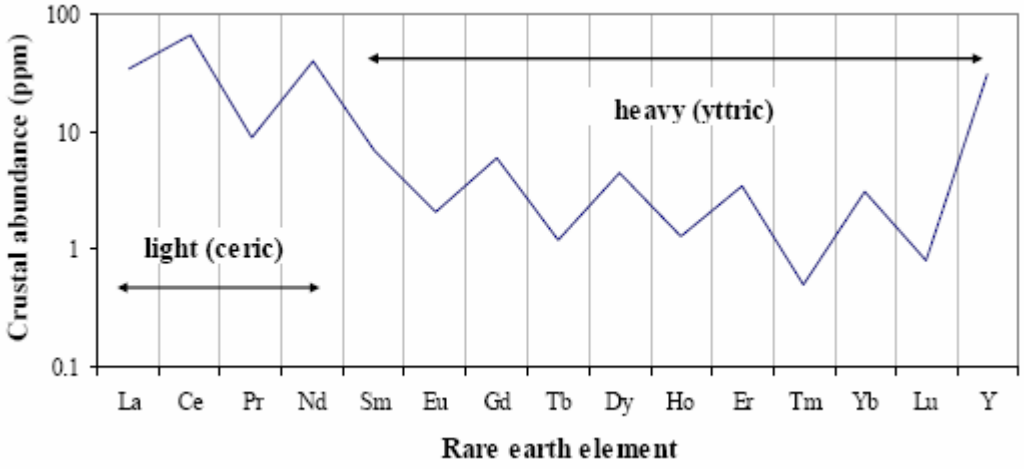

Fig. 54: Relative abundance of rare earth elements in the earth's upper continental crust

The relative abundance of the rare earth elements in the earth's upper continental crust is shown in Figure 54, some of the largest deposits of which are found in China, making it the dominant global supplier of rare earth oxides and metal today. Neodymium is one of the most abundant of these elements, its concentration varying somewhat with the type of ore. About 90% of the rare earth ore ("REO") from China is of the bastnaesite type mined in Baotou, Inner Mongolia and in Sichuan province. Bastnaesite from these regions is relatively rich in the light rare earths most commonly used in magnets, and contains about 14% neodymium oxide. But China has been implementing a strategy to support the development of its own downstream rare earth industries, such as NdFeB magnets, and to conserve its natural rare earth resources. It is doing this by tightening control over the rare earth oxides and metals that it exports, through the imposition of higher export duties and stricter export quotas. For 2008, the new tariffs on exported neodymium and dysprosium are 15% and 25% respectively, and the quota for all rare earth oxides and metals is only 22,780mT, about half the amount it exported the previous year; only 23 Chinese companies are now approved exporters, down from 41 in 2007. By taking these and other

measures, the Chinese government has demonstrated its desire and ability to stabilize rare earth prices, albeit at relatively high levels.

Almost *all* of the neodymium oxide being produced today is used in permanent magnets rather than other products The total demand for REO is expected to rise at a rate of around 10% per year, but considering the major applications for all the other rare earth elements that exist in the ore, it is the demand for permanent magnets and neodymium oxide that will continue to drive the supply gap for the next few years at least. Because additional REO must now be produced just to satisfy the market for magnets, the price of neodymium will have to bear an increasing share of the REO refining cost. Further complicating matters, almost all the neodymium metal exported from China now goes to customers in Japan, so Japanese producers of rare earth alloy and magnets are investing in new plants within China itself as a hedge against China's export restrictions. Some of the additional demand will be met from new mines located elsewhere than China, most notably Mountain Pass in California, which is resuming processing its bastnaesite ore, and Mt. Weld in Western Australia, which will be producing a monazite ore that is slightly richer in neodymium oxide (about 18.5%). Nevertheless, a significant part of the future supply gap will still have to be met from China. All of the foregoing, coupled with the weakened U.S. dollar against the Yuan, suggests that high prices for rare earth raw materials have now become the status quo.

After seeing the prices of rare earths fall to and remain at historical lows throughout the first half of this decade, the various measures taken by the Chinese government have driven these prices substantially higher and appear to have stabilized them here at least for the past twelve months. These price trends[8] are shown for neodymium metal over the past several years in Figure 55 and in more detail for the last couple of years in Figure 56.

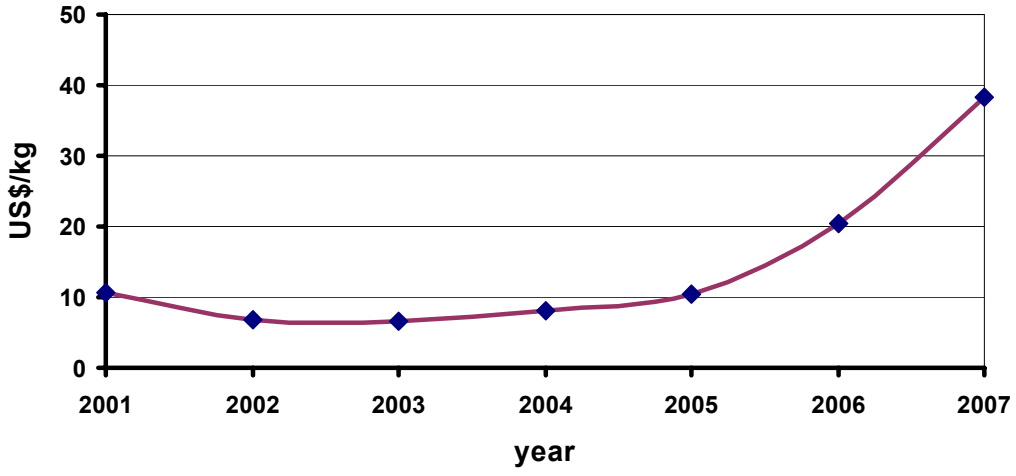

Fig. 55: Annual price trend for neodymium metal

[8] Metal Pages Ltd.: www.metal-pages.com

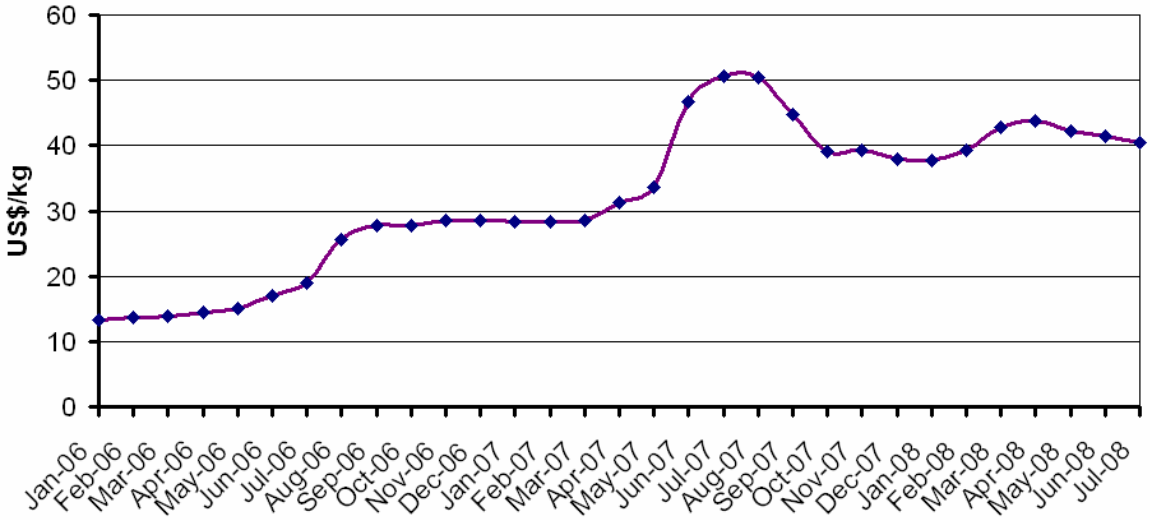

Fig. 56: Recent monthly price trend for neodymium metal

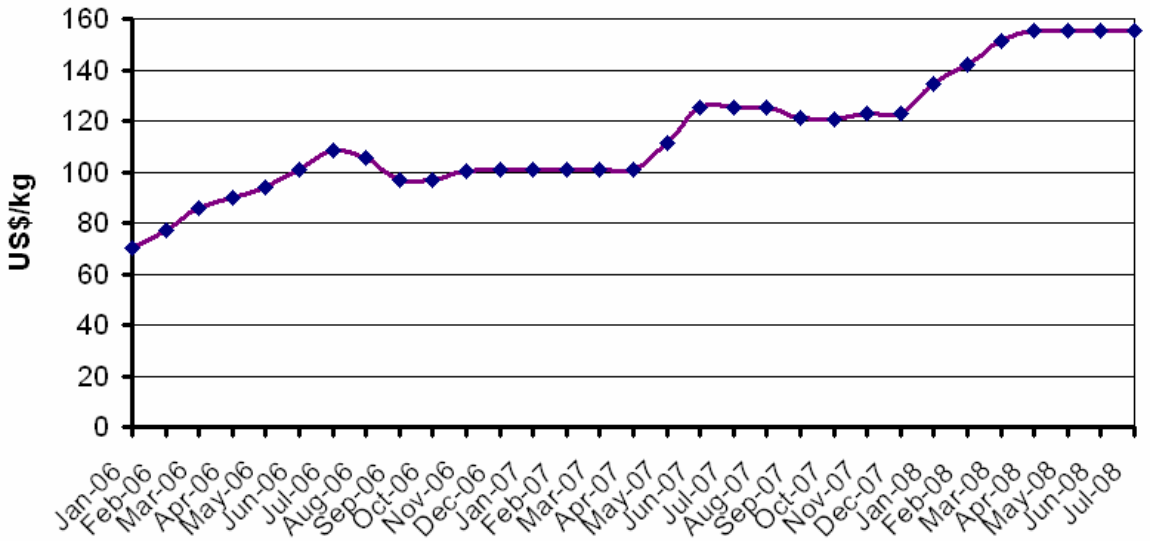

Fig. 57: Recent monthly price trend for dysprosium metal

The ores which contain heavy rare earths such as dysprosium are much less abundant than those producing light rare earths, the most productive source today being from ionic clay found in Jianzxi, Southern China. But as with neodymium, the Chinese government's measures have driven all rare earth prices substantially higher, dysprosium leveling off recently at around $155/kg as shown[8] in Figure 57. In addition to the factors already mentioned for Chinese rare earths, the price of dysprosium can also be affected by local controls in specific regions, an example of which occurred in mid-2007 when heavy rare earth production was temporarily suspended in areas of Jianxi province to counter weak demand.

To meet the demands of major new automotive applications such as motors for hybrid electric vehicle drives, dysprosium is substituted for some of the light rare

earth neodymium in the composition to improve the magnet's intrinsic coercivity and hence provide resistance to demagnetizing fields at elevated temperatures. 4.5wt% of dysprosium provides the N30UH grade magnet with sufficient H_{ci} to meet the demands of our IPM motor application. But as we saw in Table 4, an N35SH grade would provide higher B_r and lower H_{ci}, and its composition has less dysprosium (4.0wt%) and hence lower raw materials cost. So is it worthwhile switching to an N35SH grade, say? The problem is that the significantly lower intrinsic coercivity of the SH-grade will require its resistance to demagnetization at this temperature to be compensated by additional magnet thickness, and this extra magnet volume would actually raise its raw materials cost by about 16%. At least at today's prevailing prices for rare earth elements, the required resistance to demagnetization for an NdFeB magnet should be achieved by selecting the grade which achieves its smallest possible thickness, regardless of the dysprosium content which provides this, as we have done with our selections for this IPM motor.

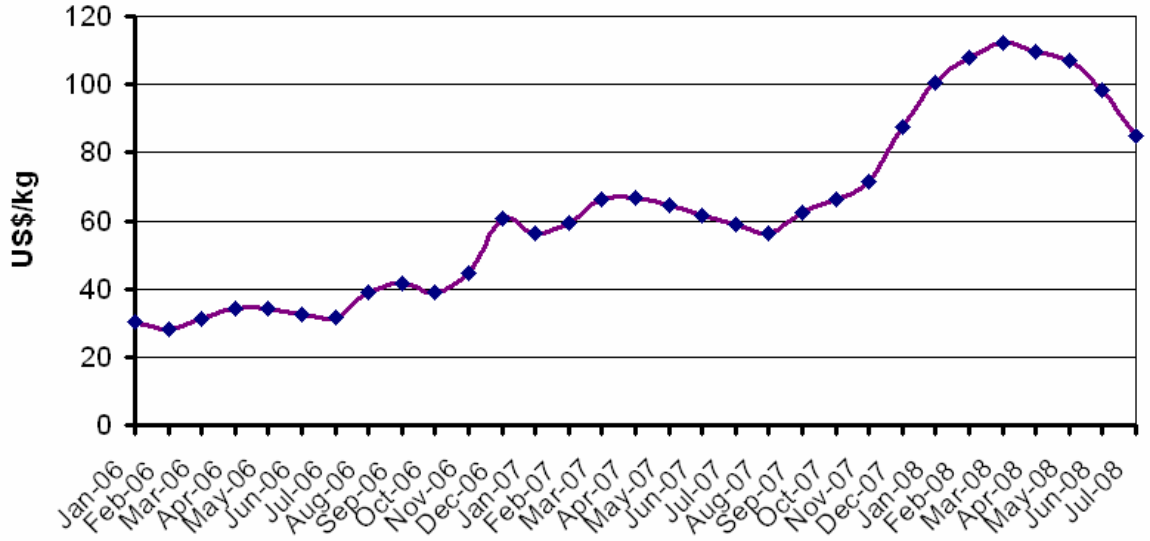

Fig. 58: Recent monthly price trend for cobalt

Cobalt is an equally valuable component of an NdFeB composition, in which it is substituted for some of the iron to provide higher temperature stability and improved corrosion resistance. It also enhances the magnet's flux density but reduces H_{ci}, partially offsetting that benefit of dysprosium. Having cost as little as $15/kg several years ago, it peaked at around $110/kg earlier this year due to short supply but has subsequently begun falling as shown[8] in Figure 58. Unlike the rare earths, cobalt is just a bi-product of nickel and/or copper which is mined mainly in Africa, where many new production facilities are planned to come on-line over the next few years (mainly in the Democratic Republic of Congo). A world supply surplus of cobalt is projected for next year[9], followed by a continued downward price trend to around $25/kg by 2015. Our N30UH grade sintered

[9] "Cobalt prices to remain high in the short term but could fall to $10-12/lb by 2015", May 15, 2008, Metal Pages Ltd.: www.metal-pages.com

magnet contains 2wt% of cobalt, which is generally a sufficient amount for its beneficial effects to be realized without degrading H_{ci} too much. The MF25 grade compression-molded NdFeB magnet uses no cobalt and yet achieves a much lower partial substitution of dysprosium.

Quotations for the N30UH and MF25 magnets were obtained in July this year from the companies who are exclusively licensed to import products to the United States from the producers we have identified: Energy Conversion Systems for San Huan, and Magnet Applications for Aichi Steel. The salient points from each quotation are as follows:

N30UH grade sintered NdFeB magnets:

- Each part (Figure 49) will be made from two 1.7" long magnets comprising the 3.4" total length;
- Pricing was based on an exchange rate of 6.86 RMB/US$;
- Price includes all tooling costs;
- Parts are imported from China and price is FOB El Paso, Texas;
- At 7,200,000 parts per year, part price is $1.646 each.

MF25 grade compression-molded NdFeB magnets:

- Each part (Figure 53) will be made from two 1.7" long magnets comprising the 3.4" total length;
- Compound is imported from Japan, compression-molding (pressing and alignment) performed in North America;
- Tooling costs will be $90,000, which if amortized over just one year only amounts to $0.45 per motor;
- At 2,400,000 parts per year, part price is $4.50 each (plus tooling).

Table 7: Costs of certain anisotropic NdFeB magnets

Magnet grade:	N30UH	MF25
Magnet raw materials price ($/kg):	21.82	12.27
Parts per motor:	36	12
Magnet part price ($):	1.646	4.50
Total magnet price per motor ($):	59.26	54.45
Magnet raw materials price per motor ($):	14.18	17.06
Magnet process cost per motor and margin ($):	45.08	37.39

Using the compositions given in Table 6 and prices corresponding to the dates when these quotations were prepared, we can compare the magnet costs as in Table 7. The cost of raw materials per kilogram for the N30UH grade sintered NdFeB magnets is significantly greater than that for the MF25 grade compression-molded NdFeB magnets, due most significantly to the former having much higher dysprosium content, and also to its cobalt and higher neodymium. But as given in Table 5, the greater magnet weight in the bonded

magnet motor tips the balance slightly in favor of the sintered magnet type when their raw materials are totaled for a whole motor. Nevertheless, the total quoted magnet price per motor is about $5 cheaper for the bonded solution over the sintered one, the difference widening further when the costs of processing these two types of magnet are compared. This favorable result for the compression-molded anisotropic magnet is due its powder being amenable to quite common compounding and molding techniques, and to each pole arc being made from one piece rather than three. Aichi's relatively complex powder preparation process is apparently not detrimental to the overall process cost.

Fig. 59: Recent monthly price trend for copper

A requirement for this IPM motor is that the total cost of the electromagnetic "active materials" referenced in Table 1 should not exceed $176. These materials consist of the stator core, rotor core and stator winding in addition to the magnets, weights of which were listed in Table 5 for both new versions of the motor design. The rotor and lamination stacks may be taken together since they would be stamped from the same steel sheets, and since they are virtually unchanged from the original UQM design, their cost may be estimated for an annual production quantity of 200,000 units from the manufacturing cost data in the UQM Final Report[2]. The price of copper for the stator winding is readily available from various financial publications[10], its fluctuation over the past year being shown in Figure 59. To be consistent with the other materials pricing, we shall use the price of copper as of July 31st which was $3.64/lb = $8.01/kg. As shown in Table 8, both new IPM motor designs using N30UH grade sintered NdFeB magnets and MF25 grade compression-molded NdFeB magnets meet the target cost for electromagnetic "active materials" of <$176.

[10] The Wall Street Journal: www.wsj.com

Table 8: Costs of active material components

Part description	Cost of parts/unit ($)	
	New design, sintered NdFeB	New design, compression-molded NdFeB
Magnets:	59.26	54.45
Stator winding (copper):	31.16	31.16
Stator & rotor laminations:	82.50	78.10
Total cost of active materials:	172.92	163.68

4.4: PRICE PERFORMANCE

Figure 15 compared the magnetic properties of all types of commercial NdFeB permanent magnets, which illustrated quite clearly the significant performance advantages that anisotropic sintered and bonded NdFeB offer over ceramic ferrite. Subsequent design analyses and cost comparisons have shown that compression-molded NdFeB is indeed comparable and very competitive with sintered NdFeB magnets for this IPM motor application.

Another useful comparative measure is *price performance*, which introduces pricing information together with magnetic properties for each of the different magnet types. *Price performance* for a magnet is defined as price per $(BH)_{max}$ with units $/kg/MGOe. Using $(BH)_{max}$ for comparison purposes is appropriate because this is the quantity most commonly used to rate a permanent magnet material, providing a measure of the best combination of a magnet's capacity to produce flux (B) and its capacity to deliver it to an air gap (H). Furthermore, the B x H product is indeed a direct measure of the energy available per unit volume of a magnet, actually being 2x this amount. It provides a particularly effective comparison when the materials all have high coercivity, which leads to approximately linear demagnetization characteristics through their maximum energy points and below – this is the case with most ferrite and rare earth magnets, whether sintered or bonded. Price performance can be plotted against any suitable variable, but magnet price ($/kg) is probably of greatest interest since this has experienced much greater fluctuations recently than have the magnets' technical properties.

Because a magnet's price and properties vary significantly with both its process method and its exact composition, there is a wide variety of commercial grades within each magnet class, and a relatively large area is spanned for each type in the price performance diagram of Figure 60. The high dysprosium content of our chosen N30UH material is needed to give it the resistance to demagnetization required for our demanding application, which makes this a relatively high performance grade of sintered NdFeB magnet with a per unit price towards the

high end of the range for this type. If price performance ($/kg/MGOe) is a measure of the value of a magnet, then Figure 60 shows that anisotropic bonded NdFeB provides very comparable value to anisotropic sintered NdFeB. Since our chosen MF25 material is the highest energy grade of compression-molded NdFeB, its value lies at the high end of the range for this type (low $/kg/MGOe), and better than that for N30UH grade sintered. We have previously dismissed isotropic bonded NdFeB magnets for failing to meet the performance requirements of the IPM motor, and as evidenced in Figure 60, their much lower energy also results in much worse (higher) price performance. Anisotropic ceramic ferrite is also shown in Figure 60 for comparison, but while it offers very good price performance value, its limited energy will also exclude it from this application.

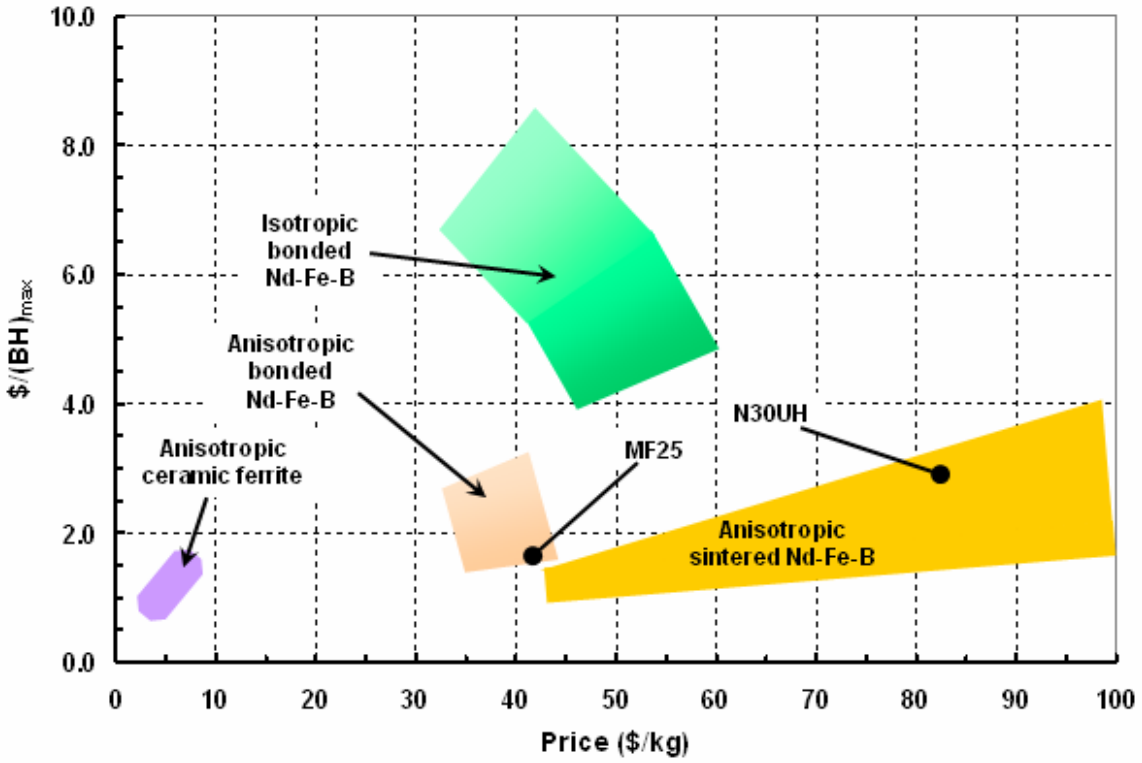

Fig. 60: Price performance of various magnet types

5: FUTURE SCENARIOS

5.1: PROSPECTIVE MATERIALS

Having shown that the requirements for this IPM motor specified in Table 1 can be achieved either with N30UH grade sintered NdFeB or with compression-molded NdFeB using MF25 grade powder, the next question is whether any other grades of either material can meet the requirements with improved price and/or performance? As we have seen, providing sufficient resistance to demagnetization at high temperature (in this case 160°C) has already driven the price of our two chosen grades towards the high ends of their respective ranges.

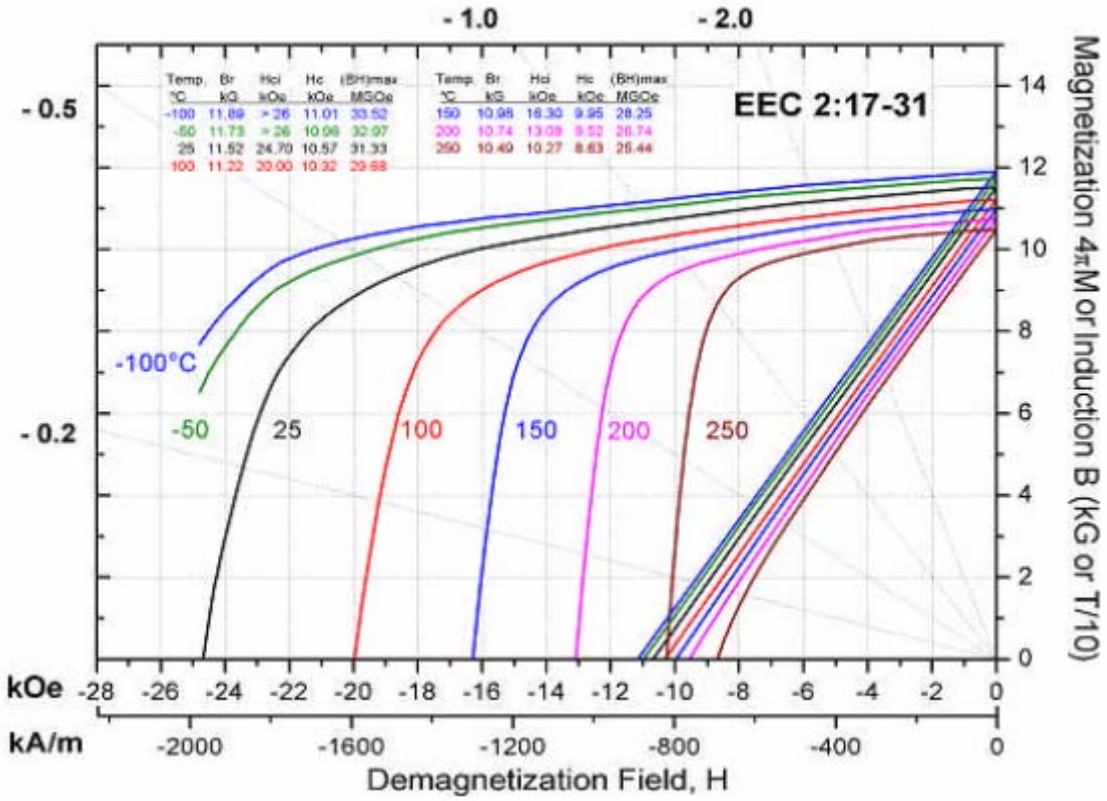

Fig. 61: Demagnetization characteristics of Electron Energy EEC 2:17-31 grade sintered SmCo

Sintered samarium-cobalt (SmCo) magnets still fill an important niche in applications which require excellent stability at high temperature. Just as we have noted that the price of neodymium will have to bear an increasing share of the REO refining cost to satisfy the growing market for magnets, a surplus of the other rare earths is created leading to a renewed interest in samarium metal and SmCo magnets. The most common of these magnets evolve from the Sm_2Co_{17} phase, though this formula changes somewhat to compensate for evaporation of samarium during the production process. The best magnetic properties are

achieved with substitutions of other transition metals (Fe, Cu, Zr) in an alloy such as $Sm(Co_{.60}Fe_{.31}Cu_{.05}Zr_{.02})_{7.9}$, typified by the EEC 2:17-31 grade material made by Electron Energy Corporation[11]. This magnet has room temperature $(BH)_{max}$ and H_{ci} of 31 MGOe and >20 kOe respectively, which is very comparable to the magnetic performance of the N30UH grade NdFeB magnet that we have chosen. But a SmCo magnet will inevitably perform better at high temperature, and as shown in Figure 61, this grade has an H_{ci} at 160°C which far exceeds the value of –9400 Oe achieved by N30UH.

Table 9: Compositions of certain rare earth alloys

Anisotropic magnet type	Grade	Composition (wt%)					
		Nd	Dy	Sm	Co	Fe	B
Sintered NdFeB:	N30UH	31	4.5		2	61.5	1
Sintered SmCo:	EEC 2:17-31			11.2	53.3	27.5	

Using the compositions given in Table 9 and prices at corresponding dates, we can compare the cost of raw materials per kilogram for these two types of sintered rare earth magnet. The raw materials for N30UH grade NdFeB magnets cost $21.82/kg as before, while those for EEC 2:17-31 grade SmCo magnets cost $52.86/kg. The high cost of sintered SmCo is due almost entirely to the very high content and current price of cobalt, on which basis it is not currently competitive with sintered NdFeB. However, under the assumption that rare earth prices remain unchanged, cost parity between these two grades is achieved if the price of cobalt falls to $36/kg, and as we have already noted, it has been projected that cobalt will continue its downward price trend to around $25/kg by 2015.

Ames Laboratory at Iowa State University has focused on developing an alloy with improved temperature stability for use in bonded magnets. We have already noted that dysprosium (Dy) may be substituted for some of the neodymium in a $Nd_2Fe_{14}B$ composition to improve the magnet's H_{ci} and hence provide resistance to demagnetizing fields at elevated temperatures. But this benefit has heretofore only been achieved using relatively expensive rare earth elements, so Ames has also employed a partial substitution of yttrium (Y) which is one of the most abundant of the rare earth elements as was shown in Figure 54. Y comprises about 65% of the REO in the ionic clay from Jianzxi, Southern China (as already mentioned the most productive source of Dy), and about 60% of the xenotime type of REO which is mined in Guangdong, China and Lahat Perak, Malaysia. The Ames alloy also includes cobalt in partial substitution for some of the iron, which enhances the magnet's flux density but reduces H_{ci}. The objective is to optimize the components of $[Nd_x(YDy)_{.5(1-x)}]_{2.2}Fe_{14-y}Co_yB$ alloy for high

[11] J. Liu and M. Walmer, "Designing with high performance rare earth permanent magnets", *18th Workshop on High Performance Magnets and their Applications*, pp. 630-636, August 2004, Annecy (France).

temperature stability with smaller *reversible temperature coefficients* of B_r (α) and H_{ci} (β).

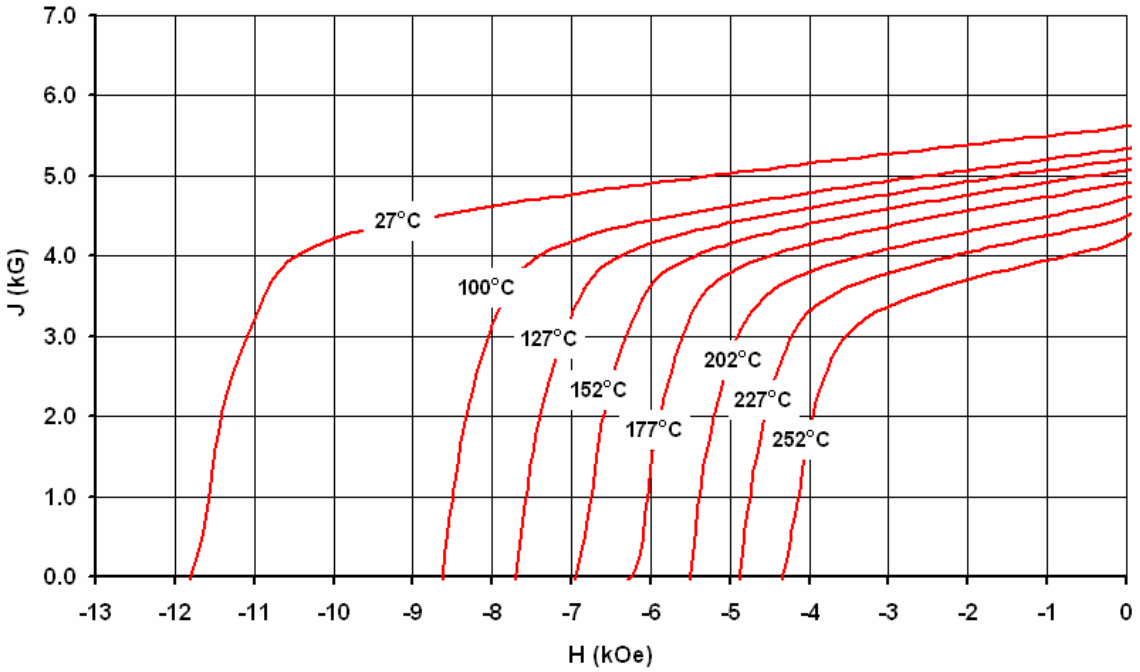

Fig. 62: Intrinsic demagnetization characteristics of WT096 grade NdFeB, compression-molded at 78.5vol%

Ames alloy grade WT096 has been melt spun and milled into isotropic powder, and if made into a bonded magnet by compounding and compression-molding, it would exhibit the projected intrinsic demagnetization characteristics shown in Figure 62. In comparison to a comparable compression-molded magnet made from the commercial isotropic MQP-14-12 grade NdFeB powder described earlier (Figure 37 for its injection-molded characteristics), the WT096 magnet would exhibit comparably good intrinsic loop squareness over the temperature range of interest, about 10% lower B_r but almost identical H_{ci} at 160°C. In comparison to the compression-molded magnet made from commercial anisotropic MF25 powder (Figure 25 for its characteristics), the WT096 magnet would exhibit far superior intrinsic loop squareness over the temperature range of interest and about 20% higher H_{ci} at 160°C; these attributes amount to much better temperature stability with much greater margin above 160°C. But while the *anisotropic* MF25 magnet has a room temperature B_r of 10,840 G, the *isotropic* WT096 magnet would only achieve 5,640 G. If it were possible to develop grain alignment and turn the WT096 alloy into an *anisotropic* powder, it could potentially double its B_r and then be preferable to MF25 in all respects as a compression-molded magnet for the IPM motor.

Using the compositions given in Table 10 and prices at corresponding dates, we can compare the cost of raw materials per kilogram for these three bonded NdFeB magnet alloys. The raw materials for MF25 grade NdFeB alloy cost

$12.27/kg as before, while those for MQP-14-12 are very comparable with a cost of $11.30/kg. However, the raw materials for WT096 alloy cost $23.0/kg, which would result in about $15 being added to the magnet raw materials price per unit of the IPM motor, driven mainly by today's prices for dysprosium and cobalt. This penalty is reduced to under $10 per motor in the event that the price of cobalt does indeed fall as we have discussed to around $25/kg in the future.

Table 10: Major elements in compositions of certain NdFeB alloys

Grade	Composition (wt%)							
	Nd	Dy	Y	Co	Fe	Ti	Nb	B
MF25	23.8	1.6			73.7			0.9
MQP-14-12	26				71		2	1
WT096	12.7	5.9	6.4	8.1	64	1.6		1

More generally, prospective new materials can be identified from the basic magnetic parameters of a number of well-known theoretical alloy compositions such as those listed in Table 11, and rated against the conventional "2-14-1" crystal type of $Nd_2Fe_{14}B$. The *saturation magnetization* (M_s) is the maximum induced magnetic moment that can be obtained in a material, which correlates directly with its consequent B_r. The *magnetocrystalline anisotropy* (H_A) is the energy necessary to deflect the magnetic moment in a single crystal of the material from the easy to the hard direction, which relates to H_{ci}.

Table 11: Magnetic parameters of various theoretical alloy compositions

Crystal type	Composition	M_s (kG)	H_A (kOe)	T_c (^oC)
"2-14-1"	$Nd_2Fe_{14}B$	16.0	67	315
"2-17"	$Sm_2Fe_{17}N_x$	15.4	210	476
"1-12"	$Nd_1Fe_{11}M_1N_1$	13.3	80	367
"3-29"	$Sm_3Fe_{27.2}Ti_{1.9}N_4$	13.0	128	477
	$Nd_3Fe_{27.9}Ti_{1.1}N_{4.7}$	15.2	81	452
	$Pr_3Fe_{27.6}Ti_{1.4}N_{5.4}$	15.8	75	427

Other new materials using iron-based compositions have tended to adopt nitrogen rather than boron, nitrogen being a well-know alternative to boron for developing coercivity. While samarium-cobalt has traditionally used a Sm_2Co_{17} alloy, this same "2-17" type of composition has been adapted to samarium-iron-nitrogen as a $Sm_2Fe_{17}N_x$ alloy. Magnetic properties of this alloy have been improved to a $(BH)_{max}$ today of around 36 MGOe, slightly better that the 31 MGOe value mentioned above for Sm_2Co_{17}. But the room temperature H_{ci} is only about 10 kOe, very disappointing in comparison to its H_A of 210 kOe and much less than that required for our IPM motor, so commercial use of $Sm_2Fe_{17}N_x$ has been rather limited and has excluded all high temperature applications. A further

problem is that the inclusion of nitrogen would cause the compound to decompose at temperatures used for sintering, which precludes its application as a fully-dense magnet. So commercial use of samarium-iron-nitrogen has also been limited to blending into compound for injection-molded magnets, albeit with its $(BH)_{max}$ diluted about 50%.

The data in Table 11 and in research literature shows that "1-12" and "3-29" type compositions could have good intrinsic magnetic properties. The "1-12" type of alloy composition ($Nd_1Fe_{12}N_x$) is significantly different from the "2-14-1" type $Nd_2Fe_{14}B$, and promises a commercial advantage with clearly lower rare earth content. So far, isotropic $Nd_1Fe_{12-x}M_xN_x$ has only achieved mediocre magnetic properties, although an anisotropic ~5μm powder version was commercialized about five years' ago[12] by Shenzhen PKU Magpoles Hi-Tech Co. But the best powder from this $Nd_{7.2}Dy_{0.5}Fe_{80.8}Mo_{11}B_{0.5}N_x$ alloy has $(BH)_{max}$ of only 24 MGOe with a room temperature H_{ci} of only 9.0 kOe, so not only would the nitrogen content limit its commercial use to bonded magnets, but also all high temperature applications such as our IPM motor would be excluded. The "3-29" alloy compositions in Table 11 are also significantly different from the "2-14-1" type, though results have yet been reported that suggest a viable commercial magnet material.

For a bonded magnet to meet the performance requirements of the IPM motor, it therefore appears that anisotropic NdFeB powder must be employed, the only commercial process method today being by HDDR, and possibly the only viable type being Aichi's top "MAGFINE" grade MF25. Rapid solidification has been mentioned as the most common process to make stable NdFeB powder for subsequent compounding and molding into a bonded magnet, this stability being contingent upon the powder not being milled to single domain size as would be required for it to be anisotropic. But it is well-know that this inherently isotropic powder can be converted into anisotropic form by hot plastic deformation, so attempts have been made to modify the conventional single roller melt-spinning technique to a twin roller[13]. The idea is to create inherent anisotropy with a combination of pressure and temperature gradient during quenching of the molten alloy, which has had some success in the laboratory but has looked neither feasible nor economical for large scale production. If another commercially viable route to anisotropy is to be found, the technical challenge would be to develop grain alignment in the course of a continuous process, which may inevitably involve further modification of the alloy's microstructure.

[12] Y. Yang, B. Cheng and S. Ge, "Multielement interstitial hard magnetic material and process for producing magnetic powder and magnet using the same", *U.S. Patent 6,419,759*, July 16, 2002.
[13] T. Kuji, R.C. O'Handley and N.J. Grant, "Method for making polycrystalline flakes of magnetic materials having strong grain orientation", *U.S. Patent 5,049,335*, September 17, 1991.

5.2: INTELLECTUAL PROPERTY

In selecting a manufacturer of sintered NdFeB magnets, it was mentioned that we would choose a "licensed" supplier. By this we mean a company which is licensed by Hitachi Metals Ltd. under the NdFeB patents they inherited when they acquired Neomax Co., formerly Sumitomo Special Metals Corporation. Currently there are eleven companies worldwide that are so licensed by Hitachi, five of which are in China, none in the United States. Since the invention of NdFeB occurred almost concurrently by Sumitomo Special Metals and General Motors Corporation (subsequently Magnequench) in 1983, one would think that all of the basic patents would have expired by now, and mostly they have. The last of the Magnequench patents covering the composition of NdFeB expired in 2006, but by means of a succession of "divisions" and "continuations", there is one basic United States patent [14] held by Hitachi on the tetragonal crystal structure of $Nd_2Fe_{14}B$ which does not expire until July, 2014. Because it has active licensees of this "'651" patent, Hitachi has a history of litigation against unlicensed producers and distributors of sintered $Nd_2Fe_{14}B$ for infringement of it. It would seem that Aichi's $(Nd,Dy)_2Fe_{14}B$ anisotropic bonded magnet composition also falls under the scope of '651, although Hitachi has shown no inclination to address this matter. With regard to the $Nd_2Fe_{14}B$ compositions which are commonly used for isotropic bonded magnets, this business area is of much less interest to Hitachi than it is to Magnequench as the leading supplier of isotropic $Nd_2Fe_{14}B$ powder. So it is Magnequench rather than Hitachi that has the history of enforcement against unlicensed producers and distributors of isotropic NdFeB, a right they have recently extended to 2014 by purchasing an exclusive "field of use" license under the '651 patent — a type of license which gives the licensee the sole right to sue for infringement in the stated "field", in this case isotropic $Nd_2Fe_{14}B$. Our review of prospective materials suggests that the tetragonal structure of the "2-14-1" crystal type ($Nd_2Fe_{14}B$) will continue to prevail, in which case Hitachi's '651 patent will continue to be of interest. But '651 is a complex patent, and so far no one has demonstrated the insight or had the resources to challenge its validity.

Two other process methods have been mentioned, that apply to powder for bonded magnets. The manufacture of anisotropic NdFeB powder by HDDR was invented by Mitsubishi Materials Corporation but still forms the basis for the more complex process used by Aichi Steel. The last of these patents[15] will expire in May, 2009. The manufacture of isotropic NdFeB powder by rapid solidification was invented by General Motors Corporation and is still practiced by Magnequench, but the last of these patents[16] expires in December, 2009.

---

[14] S. Fujimura, Y. Matsuura and M. Sagawa, "Magnetic materials and permanent magnets", *U.S. Patent 5,645,651*, July 8, 1997

[15] T. Takeshita, R. Nakayama and T. Ogawa, "Rare earth-iron-boron magnet powder and process for producing same", *U.S. Patent 5,110,374*, May 5, 1992.

[16] J, Croat, "High energy product rare earth-iron magnet alloys", *U.S. Patent 5,172,751*, December 22, 1992.